NASA CR-132602

ACOUSTIC TRANSMISSION THROUGH A FUSELAGE SIDEWALL

By J. F. Wilby and T. D. Scharton

(NASA-CR-132602) ACOUSTIC TRANSMISSION THROUGH A FUSELAGE SIDEWALL (Bolt, Beranek, and Newman, Inc.) 79 p HC $4.75 CSCL 20A

N75-18971

Unclas
G3/71 12389

Prepared under Contract No. NAS1-11839 by
BOLT BERANEK AND NEWMAN INC.
Cambridge, MA 02138

for

NATIONAL AERONAUTICS AND SPACE ADMINISTRATION

TABLE OF CONTENTS

TABLE OF CONTENTS (Contd.)

1.0 INTRODUCTION

1.1 Objectives

The objectives of the study are to define an idealized fuselage sidewall structure and to construct a simplified analytical model for determining acoustical transmission from exterior to interior of a fuselage. The representation of the sidewall structure chosen for the analytical model excludes complicating effects such as cabin pressurization, acoustic transmission through windows or door seal leaks, aerodynamic excitation and structural vibration excitation of the fuselage skin.

Development of high-lift propulsion system technology has placed considerable emphasis on sound generation from the standpoint of noise in airport communities. In contrast, little or no attention has been given to the acoustic near field problems of acoustic fatigue and airplane interior noise. This inspite of the fact that potential designs for STOL and VTOL airplanes tend to have higher thrust-to-weight ratios than conventional take-off and landing aircraft, and have propulsion systems closer to the fuselage with exhaust flows sometimes impinging on the airplane structure. Preliminary studies of acoustic fatigue on VTOL[1] and on flaps of externally-blown flap systems[2,3] have been conducted recently. This present report provides an initial step in the investigation of potential acoustic problem areas associated with interior noise of STOL airplanes.

1.2 Summary

A survey of current literature indicates that published information on airplane fuselage sidewall systems and interior noise levels is minimal. Thus it will be difficult to provide a thorough validation of any analytical model for calculation sidewall noise reduction without obtaining additional data.

Published data is useful in determining typical fuselage construction characteristics and in providing validation of some items of the analytical model. Thus Section 2 of the report discusses sidewall designs, damping loss factors and interior acoustic absorption characteristics. The section also presents an outline of the structural and excitation models for analytical study. Conventional sidewall designs consist of a fuselage shell which is of skin-stringer-frame construction. The trim panels of the interior compartment form the second wall of the sidewall double-wall system, and insulation (for thermal and acoustic reasons) is placed between fuselage skin and trim. Measured damping loss factors for typical fuselage structures are sparse but indicate values in the range 0.01 to 0.1. Acoustic absorption data for the interior relies on published data for individual components which are similar in design to those used in aircraft.

The structural model chosen for study consists of a double wall system connected by line supports. The double wall has curvature in one direction but is assumed to be infinite in extent in the other direction. Diffuse acoustic plane waves are used as a representation of the excitation field.

Section 3 presents several fuselage sidewall parameters which will be used in the formulation of the analytical model. Important frequencies include the ring and critical frequencies of the fuselage skin. The fuselage skin is divided into a series of panels by the stringers and frames, and the lower natural frequencies of such panels may be important. Application of statistical energy methods to the acoustic transmission require the determination of modal densities for the fuselage structure and the acoustical spaces, and the coupling loss factors for different elements of the transmission path. These parameters are given in Section 3.

The transmission of acoustical energy through the sidewall can be considered in terms of resonant and non-resonant response. Resonant response is discussed in Section 4 and the transmission path is broken down into four sub-systems for ease of presentation. The sub-systems are:

(a) external acoustic space to fuselage skin
(b) acoustical path from skin to interior trim
(c) structural path from skin to interior trim
(c) trim to interior acoustic space

Section 5 describes the non-resonant transmission and incorporates the transmission loss and noise reduction concepts which are familiar in traditional acoustic transmission methods for infinite structures. In Section 6 the analytical methods developed in Sections 4 and 5 are compared, where possible, with existing experimental data for conventional fuselage structures. The comparison shows reasonably good agreement between theory and experiment, particularly when it is acknowledged that the experimental data is extremely limited in availability and may not be directly applicable to the analytical model, and that the model itself suffers from possible inaccuracies because of the simplifying assumptions made in the derivation process.

Finally, the analytical model is used in Section 7 to estimate the noise levels expected in an airplane with a high-lift propulsion system.

2.0 AIRPLANE FUSELAGE STRUCTURES

2.1 Conventional Sidewall Designs

The term "fuselage sidewall" will be used in the present report to identify the system composed of the load-bearing external structure, acoustic insulation and interior trim. This total system, which is essentially a double wall from an acoustic standpoint, provides the barrier between external acoustic or aerodynamic pressure fields and the passenger inside the fuselage. Although in many cases the components of the system may be selected for reasons other than acoustic, they will all have some influence on the acoustic field within the fuselage. In an ideal design the acoustic characteristics should be included in any optimization procedure. However a comprehensive approach of this type is not possible at the present time because the analytical tools have not been developed for the acoustic model. The development of such a model is the subject of this report.

Fuselage structures of current commercial passenger-carrying airplanes are of the conventional skin-stringer-frame construction. Studies of new design concepts are currently underway, using techniques such as adhesive-bonded shells[4], to reduce the total weight of the structure. However such structures have not yet been developed into flight hardware and their use in future airplane designs has not been fully accepted. Thus for the present study it is assumed that the fuselage is of conventional design. The choice has two advantages in that the analysis can be applied to current airplane data for validation and it can be used to predict the suitability of conventional structures in overcoming potential noise and vibration problems forecast for future STOL airplanes.

The skin-stringer-frame design presents the designer with several possible parametric combinations once the basic fuselage

diameter has been selected. However the parameters are not all independent. Skin thickness can be varied but the depth and pitch of the longitudinal and circumferential stiffeners will have to be determined appropriately. Local increases in skin thickness will be necessary near cutouts such as doors and windows but over large areas the thickness may be constant. The skin may be single thickness or of double thickness bonded together in a waffle-type configuration[5,6].

Longitudinal stiffeners, or stringers, may be bonded or rivetted to the skin and may be "top-hat", inverted top-hat or "zee" in cross-sectional shape[5,6,7]. Circumferential stiffeners or frames have been used with "zee" or "tee" cross-sectional shapes[5,7] and may or may not be attached directly to the fuselage skin. Direct attachment by rivets is shown in References 5, 7 and 8, but in one case[5] the direct attachment is shown only on structures below the windows. In other regions[5,6] frames are attached by brackets to stringers and do not have direct contact with the skin. Skin thickness may be increased in the neighborhood of stiffeners by machining or by bonding additional strips[5]. Various alternative designs are depicted in Figure 1, which is based on information in Reference 5.

Dimensions reported in the literature[5,7] show skin thicknesses in the range 0.039 inch to 0.045 inch, stringer pitches of 4 - 9.2 inches and frame pitches of 17 - 20 inches. The frame pitch will be dictated in part by the window pitch selected for the fuselage design. These dimensions can be taken only as a rough guide since they do not represent a comprehensive survey of current designs. There will be considerable variation from design to design and from location to location on a given design.

The interior trim provides a decorative surface for the passenger compartments. It has to satisfy requirements for stain

resistance, ease of cleaning, and fire resistance. The trim also provides a protective cover for insulation, air-conditioning ducts, etc. As a consequence the trim is often constructed from thin panels which have hard, impervious, surfaces, such as those of metal or molded glassfiber sheet. The panels are attached to supports on the fuselage frames.

From an acoustical point of view, trim panels serve two purposes. Firstly they act as the second wall in a doublewall system, thereby controlling transmission of sound from exterior to interior. Seocndly, the acoustic absorption properties play a role in determining the acoustic reverberant build-up within the interior compartment.

In practice the dimension of the gap or cavity between the external skin and interior trim is determined by the frame depth required for structural stability. The gap is used for installation of thermal and acoustic insulation and for items such as airconditioning ducts[6]. Insulation is usually in the form of glass-fiber blankets in preformed panels or enclosed in thin-wall bags. The insulation is located between frames and also provides a cap over the top of the frames[6]. Glass-fiber blankets are used because of the good thermal and acoustic characteristics, and because the material meets fire regulations provided that the correct binder material is used.

Additional materials may be used for acoustical reasons. Such treatments include damping tape which is applied to the fuselage skin[6,9,10], the tape being applied either with or without a foam layer separating the visco-elastic adhesive from the metal sheet constraining layer. Also lead-impregnated septa, such as lead-impregnated vinyl, may be inserted between layers of insulation[10,11].

The composition of a typical fuselage sidewall[11] utilizing the components of external skin, insulation and trim is shown in Figure 2. The figure contains additional items such as windows, hat racks and airconditioning ducts which introduce additional complications into the system but the basic double-wall construction is still apparent.

2.2 Acoustic Characteristics

The main objective of the study is to determine the reduction in acoustic energy during transmission from exterior to interior. In traditional acoustic terms this reduction is referred to as the noise reduction (NR) of the sidewall. The noise reduction is the net effect of the transmission loss (TL) of skin panel and the trim, and the acoustic absorption of the wall cavity and the interior acoustic space. Experimental data for the noise reduction, transmission loss or interior space absorption are almost non-existent in the open literature but general trends can be estimated.

Measured transmission losses for an aircraft fuselage skin alone, and for the sidewall system are given in Reference 12. Since the transmission loss does not take into account the reverberant build-up inside the fuselage it will be larger than the associated noise reduction. Using the transmission loss data[12] and unpublished data for conventional airplane structures with radii in the range 100 inches to 150 inches, the noise reduction spectrum shown in Figure 3 has been constructed for unpressurized fuselages which are completely furnished. For the complete fuselage, the external noise source was the propulsion system, which provides a spatially non-homogeneous pressure field on the fuselage.

At low frequencies below about 200 Hz the noise reduction spectrum appears to be essentially independent of frequency. However at higher frequencies the noise reduction of the sidewall increases at approximately 10 dB per octave.

It should be emphasized that the spectrum in Figure 3 is no more than a rough guide, since it is based on sparse data under conditions which were not necessarily well controlled.

Acoustic absorption data are not available for typical airplane interiors but an estimate of the absorption can be obtained from published data for similar materials. On this basis an estimated absorption spectrum is determined in Appendix A and the resulting values are shown in Figure 4. The figure shows the predicted spectrum as a probable range of values based on alternative distributions of absorptive material on the fuselage sidewall and ceiling trim panels. Such distributions can vary considerably from one airplane design to another.

2.3 Damping Loss Factors for Fuselage Structure

Damping of the structure plays an important role in determining the skin resonant response to acoustic excitation. Unfortunately damping loss factors for fuselage structures are not known with any high degree of confidence and it is possible, in general, to estimate only typical ranges of values. A short survey of published information will provide an indication of the damping loss factors likely to be encountered in practice. The measurements were all made under ambient conditions (i.e. not in vacuo) and include contributions from acoustic radiation damping. However in most circumstances the radiation damping can be neglected. The main exception to this rule is when data are obtained from progressive wave ducts. In such cases the acoustic damping at low frequencies can be high and significantly influence the data.

Laboratory measurements[13,14] of the damping of single panels show very low loss factors in the range 0.002 to 0.016. When stiffeners were added the damping loss factors increased to 0.004 to 0.070[15,16,17]. Similar damping loss factors were measured on typical aircraft structures[9,8,18] with values in the range 0.022 to 0.08.

Recent measurements by Hay[19] on rivetted, welded, etched and honeycomb panels show a wide variation in loss factors ranging from 0.004 to 0.15, centered at approximately 0.02. However since these particular measurements were made in a progressive wave duct the high loss factors may include significant acoustic damping contributions.

Empirical relationships have been fitted to the experimental data [13,17,19] indicating that the lose factor η is inversely proportional to frequency f

$$\eta = \beta/f$$

where β has values in the range $1.9 \leq \beta \leq 7.5$. An exception to this trend is shown in some of the data for honeycomb structures[17] where η is essentially independent of frequency.

2.4 Analytical Model for Sidewall

The typical fuselage sidewall described in a preceding section provides numerous paths for acoustic and vibration transmission. A detailed analysis of all possible paths is outside the scope of the present study. Thus a simplified model is proposed for the sidewall. The model will include the fuselage skin, stringer, frames, insulation and interior trim, but will exclude the complicating effects of windows and doors. The stringers and frames will be represented as periodically-spaced line supports; the torsional and bending stiffnesses will be neglected. Fuselage curvature will be included but the cylinder will be assumed to be infinite in extent.

In practice the skin and stiffeners will have steady-state stresses induced by fuselage bending about the wing support and by fuselage pressurization. These stresses will be neglected. Omission of the stresses is not too important when acoustic excitation is

being considered at take-off and landing conditions, since the fuselage is not pressurized. However in cruise, when aerodynamic excitation such as that due to the turbulent boundary layer becomes significant, the fuselage will be pressurized and the static pressure differential will have important influence on sidewall response. If the analytical model is used to predict transmission of propulsion system noise through the sidewall during cruise then the inaccuracies introduced by neglecting pre-stresses should be recognized

The double-wall sidewall system will assume that skin and trim are rigidly attached to the frames. This is an adequate representation of skin-frame junction, even if the contact is through the stringer, but will be a poorer representation of the connection between frame and trim where vibration isolation mounts of some form may be used. However the characteristics of such mounts are not known and their inclusion is left for subsequent, more detailed, analyses. The insulation between fuselage skin and trim is assumed to be in the form of glass-fiber blankets since insluation of this type is in general use. Additional types of insulation using damping tape, impervious septa etc. can be included in later analyses.

An energy flow diagram for the analytical model is shown in Figure 5. There are two transmission paths, one being structural via the frames and the other acoustical through the cavity between the skin and trim panels.

2.5 Analytical Model for Excitation

The present study is considering acoustic excitation of the fuselage structure, the noise sources being the propulsion system or the high-lift propulsion system. Aerodynamic excitation such as impingement of the propulsion system exhaust or turbulent boundary layer pressure fluctuations are excluded.

As a first approximation the excitation field can be assumed to consist of a series of acoustic plane waves incident on the fuselage structure at different angles of incidence. The angles will be dependent on the relative locations of the effective sources and the structural region under investigation. For a given frequency the effective noise source will be distributed over a finite volume with the consequence that the plane waves at that frequency will be incident on the fuselage over a range of values. Thus the response of the fuselage skin panels to the acoustic excitation can be calculated by integration over the finite solid angle of incidence.

However the process can be simplified with only a small loss of accuracy. Franken and Lyon[20] have compared estimates of the vibration of Titan missile skin panels for reverberant and traveling wave acoustic excitation. The results indicate that over most of the frequency range the differences between the two estimates are less than 1 dB. Exceptions occur for the first few modes of the skin where the estimated response to traveling waves is up to 5 dB higher than that for reverberant excitation. Estimates for spacecraft cylindrical structures[21] indicate differences of less than 1 dB except near the ring frequency where the difference between the estimates was about 3 dB. On this basis a reverberant acoustic field will be assumed for the present study, as a model for the propulsion sound field on the structure. The model can be refined, if necessary, in subsequent studies.

3.0 FUSELAGE SIDEWALL PARAMETERS

3.1 Important Frequencies

Two frequencies are important in the present analysis. They are the ring frequency and the critical frequency associated with the fuselage skin.

The ring frequency f_r is a function of the radius of curvature of the fuselage and the material of the structure. The frequency is given by the equation.

$$f_r = \frac{c_L}{2\pi R} \quad \text{Hz} \tag{1}$$

where R is the fuselage radius and c_L is the wave speed for longitudin waves in the fuselage structure

$$c_L = \sqrt{\frac{E}{\rho(1 - \sigma^2)}} \tag{2}$$

In equation (2) E = Young's modules
σ = Poisson's ratio
and ρ = Mass density of the material.

The ring frequency is the natural frequency of the extensional or "breathing" mode of vibration[22] of a complete circular ring whose thickness in the radial direction is small compared to the radius R. By the same token it is the assymptotic value of the natural frequency for mode of order n = 0, as $\frac{L_x}{mR}$ tends to zero[23], where L_x is the length of the cylinder and m is the mode order in the axial direction. The ring frequency provides a boundary above which the curvature of the fuselage may be neglected when considering the vibration characteristics.

Critical frequency f_c is the lowest frequency at which acoustic coincidence occurs. It is the frequency at which the flexural wavelength in a flat plate is equal to the acoustic wavelength, and for the fuselage skin

$$f_c = \frac{\sqrt{3}\, c_o^2}{\pi h c_L} \quad \text{Hz} \tag{3}$$

where h is the skin thickness and, c_o is the acoustical velocity in the surrounding space.

Other frequencies which may enter into consideration are the natural frequencies of an individual panel of the fuselage skin. Such a panel may be defined, for example, by adjacent frames and stringer. The equation for natural frequencies of a rectangular panel, curved in one direction and having simply-supported boundaries, is

$$f_{mn} \doteq \frac{\pi^2 E h^2}{48(1-\sigma^2)\rho}\left(\frac{m^2}{L_x^2}+\frac{n^2}{L_y^2}\right)^2 + \frac{E m^4}{4\pi^2 R^2 \rho L^4}\left(\frac{m^2}{L_x^2}+\frac{n^2}{L_y^2}\right)^{-2} \tag{4}$$

Although the fuselage skin panels do not have ideal simply-supported edges the equation is probably adequate for present purposes. As an example equation (4) has been used to calculate natural frequencies of fuselage skin panels described in References 18 and 24. Assuming the circumferential mode order to be unity, ie n = 1, the modal natural frequencies were calculated and plotted in Figure 6 in terms of the wavelength component λ_x in the axial direction. The calculated results are compared with measurements on an airplane fuselage[24] at locations along a panel centerline where the mode of order n = 1 may be the dominant mode. There is found to be reasonable agreement between measurement and prediction.

3.2 Structural Modal Densities

The resonant response of a cylinder can be considered in three frequency regimes, with the ring and critical frequencies forming the regime boundaries. In the frequency range $f>f_c$ only acoustically fast (AF) modes will be present and in the range $f_c>f>f_r$ only acoustically slow (AS) modes occur. However, in the lowest frequency regime, $f_r>f$, both AF and AS modes will exist. It is assumed here that $f_c>f_r$, a condition which exists in airplane fuselage structures.

Statistical energy analysis nethods for resonant response utilize the concept of modal density for the acoustically fast and slow modes. The modal density equations have been developed for a cylinder[25] and the results can be summarized here for subsequent application to the fuselage structure. Denoting the modal densities for acoustical fast and slow modes by n_{AF} and n_{AS} respectively

$$n_{AF} = \left(\frac{f}{f_r}\right)^2 \left(\frac{f_r}{f_c}\right) \frac{\sqrt{3}A}{hc_L} \qquad f_r > f$$

$$= 0 \qquad f_c > f > f_r \qquad (5)$$

$$= \frac{\sqrt{3}A}{hc_L} \qquad f > f_c$$

and

$$n_{AS} = \left(\frac{f}{f_r}\right)^{2/3} \frac{\sqrt{3}A}{hc_L} \qquad f_r > f$$

$$= \frac{\sqrt{3}A}{hc_L} \qquad f_c > f > f_r \qquad (6)$$

$$= 0 \qquad f > f_c$$

The above expressions are approximate representations for the modal densities, but the equations are sufficiently accurate for most problems. More accurate values can be obtained[21] by use of Figure 7.

3.3 Acoustic Space Modal Densities

The average modal density for an ensemble of different acoustic spaces with volume V is given by[21]

$$n(f) = \frac{(2\pi f)^2 V}{\pi c_o^3} \qquad (7)$$

Equation (7) can be used for both the external and internal acoustic spaces associated with the airplane fuselage. At first sight the equation may seem to pose a problem in defining V for the external acoustic space. However the problem is overcome in the energy flow equations because of cancellation. Thus the choice of V is arbitrary for the exterior space.

When the acoustical space is small relative to the acoustical wavelength, equation (7) is no longer valid. For an acoustical cavity, of dimension L_c, in a double wall, Price and Crocker[26] show that the modal density at low frequencies ($f<c_o/2L_c$) is given by

$$n(f) = \frac{2\pi f S}{c_o^2} \qquad (8)$$

Where S is the surface area of one of the walls. At higher frequencies ($f>c_o/2L_c$) equation (7) can be used for cavity modal density.

3.4 Coupling Loss Factors

The coupling between resonant modes of a vibrating plate and tl resonant modes of an adjacent acoustic space can be described in terms of a coupling loss factor which can be written in the form

$$\eta_{AF} = \frac{\rho_o c_o \sigma_{AF}}{2\pi f \rho h}$$

or (9)

$$\eta_{AS} = \frac{\rho_o c_o \sigma_{AS}}{2\pi f \rho h}$$

for acoustically fast and slow modes respectively. The parameters σ_{AF}, σ_{AS} are the radiation efficiencies for the AF and AS modes respectively and their values can be obtained[25] from Figure 8.

For practical purposes σ_{AF} can be taken as unity in the frequency ranges $f>f_c$ and $f<f_r$. The radiation efficiency for acoustically slow modes depends on the frequency ratio f/f_c and on the parameter $\frac{Ph}{S}$ where P is the perimeter of the radiating panel of area S.

The appropriate value of σ_{AS} can be determined by means of Figure 8.

4.0 RESONANT RESPONSE

The response of a fuselage structure to acoustic excitation can be divided into two groups of modes, resonant and non-resonant. Resonant modes are those with natural frequencies within the band of excitation and non-resonant modes are those with natural frequencies outside the excitation band. Each modal group can in turn be subdivided into modes which are well coupled with acoustic waves in the adjacent spaces, and modes which are not well coupled.

In this section the sidewall resonant response equations will be developed. Non-resonant response will be discussed in Section 5.0.

4.1 Power Balance Equations

The simplified double wall system used in the study is shown in Figure 9. The figure shows a six-element system, including exterior and interior acoustic spaces. The energy flow paths, both resonant and non-resonant, are identified in Figure 10. Resonant mode coupling between skin panel and trim takes place along two paths, one path allowing acoustic transmission through the cavity and the other path having vibration transmission through the frame.

The power flow system shown in Figure 10 can be represented by a series of simultaneous equations which can be written in generalized form.

$$\left.\begin{aligned}
&P_{2AFdiss} + P_{2AF,1} + P_{2AF,3} + P_{2AF,6} = 0 \\
&P_{2ASdiss} + P_{2AS,1} + P_{2AS,3} + P_{2AS,6} = 0 \\
&P_{3diss} + P_{3,2AF} + P_{3,2AS} + P_{3,1} + P_{3,5} + P_{3,4} = 0 \\
&P_{4diss} + P_{4AF,5} + P_{4AS,5} + P_{4,3} + P_{4,6} = 0 \\
&P_{5diss} + P_{5,4AF} + P_{5,4AS} + P_{5,3} = 0 \\
&P_{6diss} + P_{6,2AF} + P_{6,2AS} + P_{6,4} = 0
\end{aligned}\right\} \qquad (10)$$

Equation (10) include non-resonant terms $P_{3,1}$, $P_{3,5}$ and $P_{5,3}$ but these can be put equal to zero when solving for the resonant response. Terms of the type P_{idiss} represent dissipation of energy due to the mechanical damping etc. in the particular element of the system. Other terms represent net energy flow from one element or group of modes to another. In some cases the modes are identified as acoustically fast (AF) or acoustically slow (AS). The presence of such modes will depend on the frequency band of interest.

Detailed solution of the simultaneous equation is outside the scope of the present preliminary analysis. Instead, the problem will be broken down into several components whose solution are more readily available.

The component solution can then be combined to give an approximate solution to the overall problem.

The six-element system can be reduced to five elements by the use of line supports to represent the circumferential frames. Then the system can be divided into five components for the resonant and non-resonant response. These are:

(a) Resonant transfer from exterior acoustic space (element 1) to fuselage skin (element 2)

(b) Resonant transfer from skin (element 2) to trim (element 4) via cavity (element 3)

(c) Resonant transfer from skin to trim via line supports

(d) Resonant transfer from trim to interior space (element 5)

(e) Non-resonant transfer from exterior acoustic space to interior acoustic space.

The first four components systems will be described in Section 4.2 through 4.5 and the non-resonant system will be described in Section 5.0. Energy flow diagrams for the component systems are shown in Figure 11.

4.2 Exterior Acoustic Space to Fuselage Skin

Power flow equations can be written separately for AF and AS modes

$$\begin{aligned} P_{2AFdiss} + P_{2AF,1} &= 0 \\ P_{2ASdiss} + P_{2AS,1} &= 0 \end{aligned} \tag{11}$$

These equations can be rewritten in terms of mean square energy

$$\begin{aligned} 2\pi f n_{2AF} E_{2AF} + 2\pi f n_{2AF} \eta_{2AF,1} \left[\frac{E_{2,AF}}{n_{2,AF}} - \frac{E_1}{n_1} \right] &= 0 \\ 2\pi f n_{2AS} E_{2AS} + 2\pi f n_{2AS} \eta_{2AS,1} \left[\frac{E_{2AS}}{n_{2AS}} - \frac{E_1}{n_1} \right] &= 0 \end{aligned} \tag{12}$$

Considering the AF modes, the time averaged vibrational energy of the fuselage skin is

$$E_{2AF} = \frac{\rho_2 h_2 S_2}{(2\pi f)^2} \langle a_2^2 \rangle_{AF} \qquad (1$$

where $\langle a_2^2 \rangle_{AF}$ is the space-time mean square acceleration for the acoustically fast modes, and S_2 is the panel area. A similar equation is obtained for the energy in the AS modes. For the exterior acoustic space the time averaged acoustic energy is

$$E_1 = \frac{V_1 \langle p_1^2 \rangle}{\rho_o c_o^2} \qquad (14$$

where V_1 is an arbitrary volume and $\langle p_1^2 \rangle$ is the space-time mean square acoustic pressure.

Substituting equation (5), (6), (13) and (14) in equation (12), and putting $\eta_{2AF} = \eta_{2AS} = \eta_2$

$$\frac{\langle a_2^2 \rangle_{AF}}{\langle p_1^2 \rangle} = \frac{2}{(\rho_2 h_2)^2} \frac{\sqrt{3}\pi}{2} \frac{\rho_2 c_o}{\rho_o c_2} \frac{\eta_{2AF,1}}{\eta_{2AF,1} + \eta_2} \qquad f > f_c$$

$$= 0 \qquad f_c > f > f_r \qquad (15$$

$$= \frac{2}{(\rho_2 h_2)^2} \frac{\sqrt{3}\pi}{2} \frac{\rho_2 c_o}{\rho_o c_2} \left(\frac{f}{f_r}\right)^2 \left(\frac{f_r}{f_c}\right) \frac{\eta_{2AF,}}{\eta_{2AF,1} + \eta_2} \qquad f_r > f$$

$$\frac{\langle a_2^2 \rangle_{AS}}{\langle p_1^2 \rangle} = 0 \qquad f > f_c$$

$$= \frac{2}{(\rho_2 h_2)^2} \frac{\sqrt{3}\pi}{2} \frac{\rho_2 c_o}{\rho_o c_2} \frac{\eta_{2AS,1}}{\eta_{2AS,1} + \eta_2} \qquad f_c > f > f_r \qquad (16)$$

$$= \frac{2}{(\rho_2 h_2)^2} \frac{\sqrt{3}\pi}{2} \frac{\rho_2 c_o}{\rho_o c_2} \left(\frac{f}{f_r}\right)^{2/3} \frac{\eta_{2AS,1}}{\eta_{2AS,1} + \eta_2} \qquad f_r > f$$

The coupling loss factors are given by

$$\eta_{2AF,1} = \frac{\rho_o c_o}{2\pi f \rho_2 h_2} \qquad (17)$$

and $$\eta_{2AS,1} = \frac{\rho_o c_o \sigma_{2AS}}{2\pi f \rho_2 h_2} \qquad (18)$$

where σ_{2AS} is obtained from Fig. 8, knowing $\frac{P_2 h_2}{S_2}$. In Eqs. (15)-(18) ρ_2, c_2, h_2 are the density, longitudinal wave velocity and thickness parameters for the fuselage skin panels.

4.3 Acoustic Transmission Coupling to Trim via Cavity

The energy flow path from fuselage skin to trim via the double wall cavity is shown diagrammatically in Figure 11(b). Acoustically fast and slow modes may be present in both the skin and trim panels. If both panels are of the same material the ring frequencies will be approximately equal. However in general the critical frequencies will be different for the two panels.

Power balance equations for the acoustic transmission path are

$$
\left.
\begin{aligned}
&2\pi f n_3 E_3 + 2\pi f n_3 \eta_{3,2AF}\left[\frac{E_2}{n_3} - \frac{E_{2AF}}{n_{2AF}}\right] + 2\pi f n_3 \eta_{3,2AS}\left[\frac{E_3}{n_3} - \frac{E_{2AS}}{n_{2AS}}\right] \\
&\qquad + 2\pi f n_3 \eta_{3,4AF}\left[\frac{E_3}{n_3} - \frac{E_{4AF}}{n_{4AF}}\right] + 2\pi f n_3 \eta_{3,4AS}\left[\frac{E_3}{n_3} - \frac{E_{4AS}}{n_{4AS}}\right] = 0 \\
&2\pi f n_{4AF} E_{4AF} + 2\pi f n_{4AF} \eta_{4AF,3}\left[\frac{E_{4AF}}{n_{4AF}} - \frac{E_3}{n_3}\right] = 0 \\
&2\pi f n_{4AS} E_{4AS} + 2\pi f n_{4AS,3}\left[\frac{E_{4AS}}{n_{4AS}} - \frac{E_3}{n_3}\right] = 0
\end{aligned}
\right\} \quad (19)
$$

The equations can simplified if it is assumed that there is equipartition of modal energy between AF and AS modes

$$\text{i.e.} \quad \frac{E_{AF}}{n_{AF}} = \frac{E_{AS}}{n_{AS}} \qquad (20)$$

for a given set of modes. Then equations (19) can be replaced by

$$
\left.
\begin{aligned}
&2\pi f n_3 E_3 + 2\pi f n_3 \eta_{3,2}\left[\frac{E_3}{n_3} - \frac{E_2}{n_2}\right] + 2\pi f n_3 \eta_{3,4}\left[\frac{E_3}{n_3} - \frac{E_4}{n_4}\right] = 0 \\
&2\pi f n_4 E_4 + 2\pi f n_4 \eta_{4,3}\left[\frac{E}{n} - \frac{E}{n}\right] = 0
\end{aligned}
\right\} \quad (24)
$$

In equation (21)

$$n_{2,3} = \frac{\rho_o c_o \sigma_2}{2\pi f \rho_2 h_2}, \quad n_{4,3} = \frac{\rho_o c_o \sigma_4}{2\pi f \rho_4 h_4} \tag{22}$$

$$\left.\begin{aligned} \text{where } \sigma_2 &= \frac{n_{2AF}\,\sigma_{2AF} + n_{2AS}\,\sigma_{2AS}}{n_{2AF} + n_{2AS}} \\ \text{and } \sigma_4 &= \frac{n_{4AF}\,\sigma_{4AF} + n_{4AS}\,\sigma_{4AS}}{n_{4AF} + n_{4AS}} \end{aligned}\right\} \tag{23}$$

For frequencies above the ring frequency of a given plate, equations (21) are valid since either n_{AF} or n_{AS} is zero. The approximation is of consequence at frequencies below the ring frequency, where AF and AS modes exist together. Further verification of the assumption is required.

The time-average total energies for the fuselage and trim panels are

$$\left.\begin{aligned} E_2 &= \frac{\rho_2 h_2 S_2 \langle a_2^2 \rangle}{(2\pi f)^2} \\ E_4 &= \frac{\rho_4 h_4 S_4 \langle a_4^2 \rangle}{(2\pi f)^2} \end{aligned}\right\} \tag{24}$$

Substituting in equation (21) gives the ratio of space-time mean square acceleration for the two panels.

$$\frac{\langle a_4^2 \rangle}{\langle a_2^2 \rangle} = \frac{\rho_2 h_2 S_2}{\rho_4 h_4 S_4} \; \frac{n_{2,3}\; n_{3,4}}{(n_3 + n_{3,2})(n_4 + n_{4,3}) + n_4\, n_{3,4}} \tag{25}$$

Coupling loss factors are given by equations (5), (6), (9), (22) and (23) and the relationships

$$n_2 \eta_{2,3} = n_3 \eta_{3,2}$$

$$n_3 \eta_{3,4} = n_4 \eta_{4,3} \qquad (26)$$

Structural loss factor of the trim panel is η_4 and the loss factor η_3 for the cavity is given by[26]

$$\eta_3 = \frac{S_3 c_o \alpha_3}{2\pi^2 f V_3} \qquad f < c_o/2L_3$$

$$= \frac{S_3 c_o \alpha_3}{8\pi f V_3} \qquad f > c_o/2L_3 \qquad (27)$$

where L_3 is the distance between the skin and trim, α_3 is the absorption coefficient for the cavity and S_3 is the area covered by the absorptive material. The derivation of equation (27) assumes that the absorption is distributed only over the cavity surfaces which are not transmitting sound. In the present study the absorptive material is distributed throughout the cavity volume.

4.4 Vibration Transmission to Trim via Frame

Vibration is transmitted from skin to trim by the frame attachments, although in some cases vibration isolation mounts may be used to connect trim and frame. For the present study it will be assumed that there is a rigid connection between skin and trim and that the connection can be represented by a point or line support. Vibration can then be considered on the basis of

point or line impedances for infinite plates[27]. The assumption of infinite size for the plates is acceptable because a finite plate behaves like an infinite plate when averages are performed over all modes[28].

Power balance equations for the system in Figure 11(c) can be written

$$2\pi f n_4 E_4 + 2\pi f n_4 n_{4,2} \left[\frac{E_4}{n_4} - \frac{E_2}{n_2} \right] = 0 \tag{28}$$

where E_2, E_4 are given by equation (24)

then $$\frac{\langle a_4^2 \rangle}{\langle a_2^2 \rangle} = \frac{\rho_2 h_2 S_2 n_4}{\rho_4 h_4 S_4 n_2} \frac{\eta^1_{4,2}}{\eta^1_{4,2} + \eta_4} \tag{29}$$

where $\eta^1_{4,2}$ is the coupling loss factor for the line support. The relationship for $\eta^1_{4,2}$ can be determined[27] from the point or line impedance for an infinite plate. For a point impedance (representing a stud) the input force admittance is[28]

$$Y = \frac{\sqrt{3}}{4\rho h^2 c_L} \tag{30}$$

which is real and frequency independent. If there are N studs or point impedances the coupling loss factor is

$$\eta^1_{4,2} = \frac{4N}{\sqrt{3} S_4} \left(\frac{h_4 c_4}{2\pi f} \right) \frac{(\rho_2 h_2^2 c_2)(\rho_4 h_4^2 c_4)}{(\rho_2 h_2^2 c_2 + \rho_4 h_4^2 c_4)^2} \tag{31}$$

where ρ_2, h_2, c_2 and ρ_4, h_4, c_4 are density, thickness and longitudinal wave velocity for skin panel and trim respectively.

If the frame is represented by a line support rather than a point support, the line force admittance is[29]

$$Y_\ell = Y'_\ell(1 + i) \tag{32}$$

$$\text{where} \quad Y'_\ell = \frac{1}{2\rho h}\sqrt{\frac{\sqrt{3}}{2\sqrt{2}h\pi f c_L}} \tag{33}$$

The coupling loss factor per unit length is then

$$\eta'_{4,2} = \left(\frac{2}{3}\right)^{1/4}\frac{1}{S_4}\left(\frac{h_4 c_4}{2\pi f}\right)^{1/2}\frac{(\rho_2 h_2^{3/2} c_2^{1/2})(\rho_4 h_4^{3/2} c_4^{1/2})}{(\rho_2 h_2^{3/2} c_2^{1/2} + \rho_4 h_4^{3/2} c_4^{1/2})^2} \tag{34}$$

In practice the frame is attached to the skin either along lines when there is direct rivetting to the skin, or approximately at points when attached by brackets to stringers. The trim may have point attachment through mounts. Thus the attachments are somewhere between point and line idealization. Also the frame will impose moment admittances which have been omitted from the discussion.

4.5 Trim Panel Coupling to Interior Acoustic Space

The coupling between resonant modes of the trim panel and interior acoustic space can be analyzed in terms of the acoustically fast and slow modes of the trim. The power flow equation, representing the system in Figure 11(d) is

$$2\pi f\eta_5 E_5 + 2\pi f n_5 \eta_{5,4AF}\left[\frac{E_5}{n_5} - \frac{E_{4AF}}{n_{4AF}}\right] + 2\pi n_5 \eta_{5,4AS}\left[\frac{E_5}{n_5} - \frac{E_{5AS}}{n_{4AS}}\right] = 0 \quad (35)$$

where modal densities n_{4AF}, n_{4AS} are given by equations (5) and (6), and time-average total energies E_{4AF}, E_{4AS} are given by equation (24). The time-average total energy for the interior acoustic space is

$$E_5 = \frac{V_5}{\rho_o c_o^2} \langle p_5^2 \rangle \quad (36)$$

and the loss factor η_5 for the interior space can be written as

$$\eta_5 = \frac{c_o S_5 \alpha_5}{8\pi f V_5} \quad (37)$$

where α_5 is the mean absorption coefficient for the interior space and is distributed over an area A_5. Appropriate values of α_5 for a furnished fuselage are shown in Figure 4.

If the absorption coefficient is obtained from measurements of reverberation time T_R for the enclosure, the energy absorption will include transmission out through the walls. This total absorption coefficient can be denoted by α_T and the associated loss factor is

$$\eta_{5T} = \frac{c_o S_5 \alpha_T}{8\pi f V_5} \quad (38)$$

$$\text{with } \alpha_T = \frac{17.6\pi V_5}{c_o S_5 T_R} \tag{39}$$

Equation (35) can now be written in the form

$$\langle p_5^2 \rangle = \frac{\rho_o^2 c_o^2}{\pi^2 f^2} \frac{S_4}{S_5} \frac{1}{\alpha_T} \left[\sigma_{4AF} \langle a_4^2 \rangle_{AF} + \sigma_{4AS} \langle a_4^2 \rangle_{AS} \right] \tag{40}$$

If equipartation of modal energy is assumed for AF and AS modes then equation (40) reduces to

$$\frac{\langle p_5^2 \rangle}{\langle a_4^2 \rangle} = \frac{\rho_o^2 c_o^2 \sigma_4}{\pi^2 f^2 \alpha_T} \frac{S_4}{S_5} \tag{41}$$

where

$$\sigma_4 = \frac{n_{4AF}\sigma_{4AF} + n_{4AS}\sigma_{4AS}}{n_{4AF} + n_{4AS}} \qquad \text{from (23)}$$

$\sigma_{4AF}=1$, σ_{4AS} is obtained from Figure 8 and modal densities n_{4AF}, n_{4AS} are calculated from equations (5) and (6).

In equation (41) the surface areas S_4 and S_5 are identified separately since conditions may occur where the two surfaces have to be distinguished. For example if sound is transmitted through the side walls and not through the floor then $S_4 < S_5$.

5.0 NON-RESONANT PANEL RESPONSE

5.1 Transmission Loss

Non-resonant response analysis applies to finite and infinite panels since the influence of boundaries is neglected. In the case of the fuselage skin and interior trim non-resonant response can occur in modes which are acoustically well-coupled or poorly-coupled to the adjacent acoustic spaces. The poorly-coupled modes can be neglected in practice because they make only insignificant contributions to the vibration and acoustic radiation fields.

The term non-resonant, acoustically well-coupled mode refers to response in a frequency band which is higher than the natural frequency of the mode, where the vibration wave is acoustically fast. Under these conditions the non-resonant mean square acceleration resulting from an acoustic plane wave incident at an angle ϕ can be written[21]

$$\frac{\langle a_2^2 \rangle}{\langle p_1^2 \rangle} = \frac{4}{(\rho_2 h_2)^2} \left[1 + \left(\frac{\rho_o c_o}{\pi f \rho_2 h_2 \cos \phi} \right)^2 \right]^{-1} \tag{42}$$

or, for a diffuse acoustic excitation field[21]

$$\frac{\langle a_2^2 \rangle}{\langle p_1^2 \rangle} = \frac{2}{(\rho_2 h_2)^2} \left\{ 1 - \frac{\rho_o c_o}{\pi f \rho_2 h_2} \tan^{-1} \left(\frac{\pi f \rho_2 h_2}{\rho_o c_o} \right) \right\} \tag{43}$$

The second term in equation (43) represents the acoustic radiation loading of the structure. In many practical cases of structures in air the radiation loading is small and can be neglected. Then the non-resonant response is

$$\frac{\langle a_2^2 \rangle}{\langle p_1^2 \rangle} \simeq \frac{2}{(\rho_2 h_2)^2} \tag{44}$$

For aircraft structures this is probably true at all frequencies except those at the lower end of the frequency range of interest. The mass law represented by equation (43) gives a lower bound to the response since the addition of structural damping cannot reduce the response below the mass law value (except in so far as the damping material adds mass to the structure and increases ρ_2).

The sound transmission coefficient, τ, is the ratio of power transmitted to power radiated, From equation (42)

$$\tau_{3,1} = \left[1 + \left(\frac{\pi f \rho_2 h_2 \cos\phi}{\rho_o c_o}\right)^2\right]^{-1} \tag{45}$$

which is the mass law transmission loss (e.g. Reference 30)

From equation (43), the transmission loss for a diffuse field is

$$\tau_{3,1} = \left(\frac{\rho_o c_o}{\pi f \rho_2 h_2}\right)^2 \log_e \left[1 + \left(\frac{\pi f \rho_2 h_2}{\rho_o c_o}\right)^2\right] \tag{46}$$

5.2 Noise Reduction

Considering non-resonant panel vibration only, the power flow equations can be written

$$\left.\begin{aligned} 2\pi f\eta_3 E_3 + 2\pi f n_3 \eta_{3,1}\left[\frac{E_3}{n_3} - \frac{E}{n_1}\right] + 2\pi f n_3 \eta_{3,5}\left[\frac{E_3}{n_3} - \frac{E_5}{n_5}\right] = 0 \\ 2\pi f\eta_5 E_5 + 2\pi f n_5 \eta_{5,3}\left[\frac{E_5}{n_5} - \frac{E_3}{n_3}\right] = 0 \end{aligned}\right\} \quad (47)$$

It is assumed in equation (47) that there is resonant response of the cavity. Now the noise reduction is

$$NR = 10 \log\left(\frac{E_1}{V_1}\right) - 10 \log\left(\frac{E_5}{V_5}\right) \quad (48)$$

From equation (47)

$$NR = 10 \log\left[(1 + \frac{\eta_3}{\eta_{3,1}})(1 + \frac{\eta_5}{\eta_{5,1}}) + \frac{\eta_5}{\eta_{3,1}} \frac{V_3}{V_5}\right] \quad (49)$$

The coupling loss factor can be expressed in terms of the transmission coefficients[26]

$$\left.\begin{aligned} \eta_{3,1} &= \frac{c_o S_2 \tau_{3,1}}{8\pi f V_3} \\ \eta_{3,5} &= \frac{c_o S_4 \tau_{3,5}}{8\pi f V_5} \end{aligned}\right\} \qquad (50)$$

Also the loss factor for the interior acoustic space is

$$\eta_5 = \frac{c_o S_5 \alpha_5}{8\pi f V_5} \qquad (37)$$

Price and Crocker[26] show that the loss factor for the cavity is

$$\left.\begin{aligned} \eta_3 &= \frac{S_3 c_o \alpha_3}{2\pi^2 f V_3} \quad f < c/2L_3 \\ &= \frac{S_3 c_o \alpha_3}{8\pi f V_3} \quad F > c/2L_3 \end{aligned}\right\} \qquad (27)$$

which can be written as $\eta_3 = \frac{S_3 c_o \alpha_3}{2\varepsilon\pi f V_3}$ (51)

where $\varepsilon = \pi$ when $f < c_o/2L_3$
$= 4$ when $f > c_o/2L_3$ (52)

Combining equations (27), (37), (49) - (52), the non-resonant noise reduction is

$$NR = 10 \log_{10}\left[(1 + \frac{4}{\epsilon}\frac{\alpha_3}{\tau_{3,1}})(1 + \frac{\alpha_5}{\tau_{3,5}}) + \frac{\alpha_5}{\tau_{3,1}}\right] \text{dB} \qquad (52)$$

where it has been assumed that

$$S_2 = S_3 = S_4 = S_5$$

If it is assumed that $S_4 \neq S_5$, then the noise reduction is

$$NR = 10 \log_{10}\left[(1 + \frac{2}{\epsilon}\frac{\alpha_3}{\tau_{3,1}})(1 + \frac{S_5}{S_4}\frac{\alpha_5}{\tau_{3,5}}) + \frac{S_5}{S_2}\frac{\alpha_5}{\tau_{3,1}}\right] \text{dB} \qquad (53)$$

Values for the transmission loss coefficients are obtained from equations (45) or (46). Absorption coefficients are calculated from available data or obtained from reverberation time measurements (equation (39)).

6.0 COMPARISON WITH MEASUREMENTS

It is always desirable to validate an analytical model by comparison with measurements on the corresponding practical system. In the present case, such comparisons are difficult because the published data are very sparse. For example, since no vibration data are available for trim panels, it is not possible to evaluate the individual model components which describe acoustic and vibration transmission from fuselage skin to trim. Also it is not possible to validate the model component which predicts radiation into the interior space from trim vibration. This leaves only two possible comparisons between theory and experiment:

(a) fuselage skin response to acoustic excitation
(b) noise reduction for the total sidewall system.

Both comparisons have their limitations, which will be discussed in the following sections.

6.1 Fuselage Skin Vibration

The specific interest is the evaluation of equations (15) and (16) by comparison with measurements on a typical airplane fuselage. Measurements of skin response to turbulent boundary layer and jet noise excitation have been reported [18,24] and one of the cases studied was that of jet noise excitation at take-off when the fuselage was unpressurized. This corresponds to the model used in the analysis. In particular, Figure 7(b) of Reference 24 shows the acceleration power spectral density function for a panel center point, in terms of unit excitation. The spectrum curve is reproduced in Figure 12. Measurements were made in a relatively narrow frequency bandwidth of 2.9%. As a consequence, the spectrum has an irregular shape which will not be reproduced by the analysis where spatial averaging is performed over the panel area and over a relatively wide frequency bandwidth.

Relevant parameters for the fuselage structure are [5,18,24]:

skin thickness	0.09	cm	(0.036 inch)
doubler thickness	0.09	cm	(0.036 inch)
stringer pitch	23.4	cm	(9.2 inches)
frame pitch	50.8	cm	(20 inches)
fuselage radius	1.8	m	(74 inches)

Only one value of structural damping is given in the references [18]. Here a loss factor of 0.08 is assumed for all frequencies.

Based on the data, the important frequencies are calculated to be:

ring frequency f_r = 450 Hz
critical frequency f_c = 11,620 Hz
fundamental frequency of panel $f_{1,1}$ = 90 Hz

In the last case, the natural frequency of the panel is calculated on the basis of a rectangular panel, which is simply supported at the stringer and frames. The critical frequency is calculated assuming that the mass of the doubler is uniformly distributed over the panel area.

From the above data, it is seen that resonant acoustically slow modes will be present throughout the frequency range of interest (100-5000 Hz) but that acoustically fast modes occur only at frequencies below 450 Hz. Use of equations (15) and (16) for frequency ranges $f_c > f > f_r$ and $f > f_r$ gives the calculated response spectrum shown in Figure 12. In view of the approximations involved, the agreement between theory and experiment is good. One important potential source of error arises because the excitation and response were not measured at the same location [24]. Since the jet noise spectrum is not homogeneous, the actual pressures exciting the fuselage will probably differ from those measured.

A second factor influencing the agreement between measured and predicted results is the method of measuring the excitation pressure field, which was done using flush-mounted microphones. Thus, the measured pressures would include reflection effects not included in the estimated space-averaged pressure. If pressure reflection effects were removed from the measured data, the associated spectrum curve in Figure 12 would increase by up to 6 dB, depending on frequency.

6.2 Noise Reduction for Sidewall

The noise reduction provided by fuselage sidewall and interior acoustic space can be estimated for resonant and non-resonant panel response.

Considering first the resonant panel response, the noise reduction is calculated by combining equations (15), (16), (25), and (41) for transmission via the double wall cavity, and by combining equations (15), (16), (29) and (41) for transmission via the frame. The case of vibration transmission through the frame has two alternative methods: one for point supports and one for line supports.

To estimate the noise reduction for a typical fuselage, the skin parameters are assumed to be the same as those used in Section 6.1. In addition it is assumed that the distance between skin and trim is 11.45 cm (4.5 inches), and that the trim is an aluminum panel which is 0.04 cm (0.016 inch) thick. The cavity between skin and trim panels is filled with glass-fiber blankets contained in plastic bags with a very thin wall. Mean absorption coefficients assumed for the cavity are:

Frequency (Hz)	125	250	500	1000	2000	4000
Absorption Coefficient	0.22	0.37	0.82	0.99	0.88	0.63

The cavity resonance mode defined by $c_{\ell co}/2L_3$ is 1490 Hz.

Absorption coefficients for the interior acoustic space are taken to be the mean values for the range shown in Figure 4.

Following the above procedures noise reductions calculated for resonant response of the panels exceed the empirical data of Figure 3. The comparison is shown in Figure 13. Estimates for transmission through the cavity show noise reduction values much greater than the experimental data. When transmission is through the frame, the estimated noise reductions are closer to, but still exceed, the measured results at most frequencies.

The estimates of noise reduction provided by transmission through the frame show a range of values at each frequency. The lower bound of the range corresponds to a line impedance representation and the upper bound to a point impedance representation.

Turning to the non-resonant response of the skin and trim panels, the noise reduction is calculated using equations (46) and (53). The sidewall parameters are assumed to be the same as those used in the resonant response analysis, and the mass of the glass-fiber blankets is added to the mass of the trim panel. Agreement between measurements and predictions is now much closer (Figure 14) than was the case for resonant response. The calculated noise reduction spectrum lies within the empirical data range except at low frequencies, well below the fuselage ring frequency. At these frequencies stiffness effects, not included in the non-resonant response calculations, will become dominant, and the assumptions implicit in the non-resonant response equations will no longer be valid.

Some caution has to be observed in interpreting the comparisons in too great a detail. Since the empirical data are sparse and were obtained under conditions which are not well defined, it is appropriate to consider the comparisons in Figures 13 and 14 as being only order of magnitude comparisons until further evidence is available.

7.0 PREDICTION OF STOL INTERIOR NOISE

Several high-lift propulsion STOL aircraft configurations are currently of interest to NASA, the Air Force, and the aircraft industry. Herein we use the preliminary results of this study, and small-scale test data obtained by BBN under NASA contract, to estimate the interior noise for a STOL aircraft employing one of the high-lift configurations of current interest, i.e., over-the-wing blowing (OWB). For this configuration, the engine exhaust gas exits from a nozzle positioned on top of the wing; the Cuanda effect turns the exhaust gas down over the flaps. OWB offers the potential acoustic advantage that the wing shields the core engine noise from the community and, in the case of a high-wing aircraft, from most of the aircraft fuselage. Unfortunately the flow of the turbulence in the jet exhaust over the trailing edge of the flap generates additional low-frequency noise.

Consider a high-wing USB aircraft powered with two QCSEE-engines.

Table 1 - QCSEE Engine Parameters

Thrust per engine	21,000 lbs
Fan pressure ratio	1.35
Mixed jet velocity	800 ft/sec
Mixed jet temperature	680°R
Mixed jet diameter	5.7 ft

To predict the interior noise of this aircraft during takeoff and landing, we consider three interior noise sources which are not generally important for conventional aircraft: (1) sound generated by the interaction of the jet exhaust with the flap, (2) excitation of the fuselage by the turbulence fluctuations in the jet exhaust, and (c) fuselage vibrations transmitted from the flap and wing structure. We do not consider here conventional sources of jet aircraft interior noise such as:

turbomachinery, auxiliaries, and jet exhaust at takeoff or turbulent boundary excitation of the cabin during cruise.

7.1 Prediction of Exterior Sound and Aerodynamic Pressure Spectra

The estimated aircraft exterior acoustic and aerodynamic fluctuating pressure spectra for the two-engine USB aircraft are shown in Fig. 15. These estimates were deduced from BBN 1/15 scale cold flow model data.[31] The scaling relations used to estimate the QCSEE-powered aircraft pressure levels shown in Fig. 15 are given by Eqs. 54 through 56 in which SPL and APL refer to the octave band sound-pressure-levels and aerodynamic-pressure-levels respectively and f refers to the frequency at which the peaks in the spectra occur.

$$\frac{SPL_Q}{SPL_M} \approx 10 \log\left[\frac{\rho_Q}{\rho_M}\frac{A_Q}{A_M}\left(\frac{V_Q}{V_M}\right)^6\left(\frac{R_M}{R_Q}\right)^2\right] \tag{54}$$

$$\frac{APL_Q}{APL_M} \approx 10 \log\left[\left(\frac{\rho_Q}{\rho_M}\right)^2\left(\frac{V_Q}{V_M}\right)^4\right] \tag{55}$$

$$\frac{f_Q}{f_M} \approx \frac{V_Q}{V_M}\frac{h_M}{h_Q} \tag{56}$$

In these equations the subscript Q refers to the QCSEE-powered configuration, M to the model configuration, ρ to the mixed jet density, A to the mixed flow nozzle area, V to the mixed flow exit velocity, R to the distance from the measurement point to the flap trailing edge, and h the nozzle height or diameter.

For comparison, we have used three other sources of basic data to estimate these acoustic and aerodynamic pressure spectra. Using the NASA Lewis Research Center data and prediction technique described in Ref. 32, we estimate the maximum octave band sound

pressure level 5 ft below the flap at 130 dB. Using the NASA Ames Research Center data presented in Ref. 33 we estiamte from Eq. 54 a maximum octave band level of 128 dB. These levels are to be compared with the 126 dB maximum level presented in Fig. 15. Using the results of two other BBN small-scale experimental investigations,[34,35] we estimate nearly the same aerodynamic pressure levels as those shown in Fig. 15.

The accuracy of these predictions are dependent not only on the validity of the base data but also upon the accuracy of the scaling relations. The aerodynamic pressure and sound radiated at the trailing edge of the flap depend on the flow properties at the flap trailing edge rather than the properties at the nozzle exit plane which are used in the scaling relations 54 through 56. (See, for example, Refs. 36 and 37.) For given conditions at the nozzle exit, the flow conditions at the trailing edge of the flap depend on many details: most importantly, of course, on the attachment of the flow, but also on the ratio of the nozzle height to the distance from the nozzle to the trailing edge of the flap, on the ratio of the jet density to ambient density, on forward speed, on flap turning angle, and in general on flap geometry -- such as position of the fuselage, fences, etc. We have not attempted to take account of these details in the predictions presented in Fig. 15

7.2 Fuselage Noise Reduction

The fuselage noise reduction characteristics used to estimate the STOL aircraft interior noise are shown in Fig. 16. The solid curve in Fig. 16 depicts the high-frequency estimate of fuselage noise reduction calculated in this study utilizing a model in which the inner and outer fuselage skins were represented as limp masses and the intermediate acoustic space was

represented as a resonant cavity with some absorption, see Fig. 14. In the low-frequency region where the fuselage stiffness and curvature are important, we have estimated the fuselage noise reduction for *acoustic* excitation by the short-dashed curve in Fig. 16.

The low-frequency noise reduction for *aerodynamic* excitation of the fuselage is approximately 10 dB higher than that for acoustic excitation (BBN proprietary data) as illustrated by the long dashed curve in Fig. 16. The cross-hatched region in Fig. 16 indicates measured aircraft noise reductions for acoustic excitation.

7.3 Estimate of Interior Noise

Figure 17 shows the estimates of interior noise for a USB two-engine aircraft. The interior noise estimates were calculated by combining the predicted exterior acoustic or aerodynamic fluctuating pressure levels in Fig. 15 with the appropriate estimates of fuselage noise reductions shown in Fig. 16.

The solid curve in Fig. 17 is the estimate of interior noise due to acoustic excitation of the fuselage. In Fig. 17 this estimate is compared with data for a range of existing jet aircraft, including all seats. The interior noise of the USB aircraft due to acoustic excitation is as loud or louder in the low-frequency regime, between 20 and 125 Hz, as any of the seats on any of the existing jet aircraft. In addition in a high wing USB aircraft with the flaps deployed for takeoff or landing, almost the entire cabin will be exposed to these high acoustic levels.

The dashed curve in Fig. 17 is the estimate of the USB aircraft interior noise if the jet exhaust impinges directly on the aircraft fuselage after it leaves the flaps. The dashed curve in Fig. 17 may be viewed as an upper bound in the sense that it would be unlikely and impractical to have a substantial portion of the aircraft fuselage bathed by the jet exhaust.

The dashed curve in Fig. 17 may also be interpreted as an upper bound for the third type of excitation which we have not considered per se, i.e., excitation of the fuselage by vibrations transmitted from the wing and flap structures. The fluctuating aerodynamic pressures estimated in Fig. 15 will excite vibrations of the wings and flaps. There will be some transfer function relating the vibrations of the wings and flaps to the resulting fuselage vibrations. If this transfer function were unity, one would predict that the interior noise due to this vibration transmission path would correspond to the dashed estimate in Fig. 17. In general this transfer function will be less than unity by perhaps 0-20 dB, and the interior noise resulting from this vibration transmission path might be expected to lie somewhere between the dashed and solid curves presented in Fig. 17.

These estimates of OWB aircraft interior noise should be considered as preliminary, and more refined estimates should be prepared as more data and design details become available. However, these preliminary estimates suggest that low-frequency cabin noise is a potential problem in high-lift propulsion type aircraft.

8.0 CONCLUSION AND RECOMMENDATIONS

Analysis of sound transmission through a fuselage sidewall includes both resonant and nonresonant vibration of the fuselage skin and trim panels. The simple model used in the present study represents the sidewall system as a double wall curved in one direction and infinite in the other direction. Stiffeners in longitudinal and circumferential directions are considered as point or line supports with no torsional components. Acoustic absorption is assumed to fill the cavity in the double wall, and direct structural connections between skin and trim is provided by the circumferential stiffeners.

The study considered fuselage response and sound transmission in the frequency range 100-5000 Hz. This range lies below the critical frequency for the fuselage skin with the consequence that there is poor coupling between acoustic plane waves and resonant modes of the structure, except below the fuselage ring frequency where some resonant modes will be well coupled.

Within the above constraints, the following conclusions can be drawn for acoustic transmission through the sidewall of an unpressurized fuselage:

(a) Resonant panel response coupled by acoustic transmission through the double wall cavity provides considerably more noise reduction than is observed in practice.

(b) Resonant panel response coupled by vibration through the frames provides less noise reduction than for coupling via the cavity, but at most frequencies the reduction is still greater than that observed in practice.

(c) Nonresonant panel response, coupled with resonant response of the double-wall cavity, predicts noise reductions which are similar to those measured on representative structures.

(d) At low frequencies, below about 0.5 f_r, empirical noise reduction data appear to be independent of frequency. In this frequency region panel stiffness effects are expected to become dominant and the assumptions of non-resonant motion will become invalid.

(e) At high frequencies, above the critical frequency, the resonant panel modes will become more efficient radiators and may control the noise reduction of the sidewall system. However, because the critical frequencies are high for typical conventional structures, the sound transmission at these frequencies may not be important for fuselage interiors.

The objectives of the study were to analyze acoustic transmission through a simplified sidewall system. Since the results of the study show reasonably good agreement with available experimental data, it is appropriate to extend the analysis to include additional structural factors and aerodynamic excitation. The following recommendations are made for further studies.

(a) Since low frequencies are likely to be important in STOL airplanes, the present analysis should be extended to lower frequencies by considering response at frequencies below the fundamental natural frequency of a fuselage skin panel. There are two aspects to the problem. Firstly the vibration of an individual panel will be stiffness controlled and the curvature will be important. Secondly, the motion of longitudinal stiffeners may play an important role.

(b) Acoustic excitation of the fuselage structure may be important during flight for some of the STOL configurations. Thus the influence of cabin pressurization should be studied. The pressurization will introduce membrane stresses in the fuselage skin and increase the panel natural frequencies.

Thus the low frequency response discussed in Item (a) above will be extended to higher frequencies when pressurization is included.

(c) In current high speed airliners, interior cruise sound levels are dominated by aerodynamic excitation from the turbulent boundary layer. Similar excitation will be very important in STOL airplanes during cruise and there is the additional factor that exhaust from the high-lift propulsive system may impinge on the fuselage skin. Therefore it is evident that an excitation model describing the aerodynamic pressure field on the fuselage should be a part of the sidewall noise reduction model.

(d) Reference was made in the Introduction to studies of flap vibration under direct inpingement of exhaust gases. Vibration of this type can be transmitted to the fuselage structure and then radiated as sound into the fuselage. Noise transmission of this form should be a part of the overall analytical model.

REFERENCES

1. R. Scholten "Influence of the ground on the near field noise levels of jet-supported V/STOL aircraft". Chp 2 of "Symposium on Acoustic Fatigue", AGARD-CP-113 (1973).

2. D. L. Lansing, J. A. Drischler, T. J. Brown, J. S. Mixson "Dynamic loading of aircraft surfaces due to jet exhaust impingement". Chp 3 of "Symposium on Acoustic Fatigue", AGARD-CP-113 (1973).

3. E. E. Ungar, K. L. Chandiramani, J. E. Barger "Excitation, response, and fatigue life estimation methods for the structural design of externally blown flaps". NASA CR-112216 (October 1972), (Also BBN Report 2469).

4. J. E. McCarty et al. "Advanced metallic structure: Cargo fuselage design for improved cost, weight, and integrity". AFFDL-TR-73-53 (June 1973).

5. L. D. Jacobs, D. R. Lagerquist, F. L. Gloynar "Response of complex structures to turbulent boundary layers". J. Aircraft. 7, 3, 210-219 (May - June 1970).

6. J. B. Large, J. F. Wilby, E. Grande, A. O. Andersson "The development of engineering practices in jet, compressor, and boundary layer noise" Aerodynamic Noise. Editor H. S. Ribner 43-47. University of Toronto Press (1969).

7. M. J. Crocker "The response of a supersonic transport fuselage to boundary layer and to reverberant noise". J. Sound and Vibration. 9, 1, 6-20, (January 1969).

8. B. L. Clarkson, R. D. Ford "The response of a typical aircraft structure to jet noise". J. Royal Aero. Soc. 66, 31-40 (January 1962).

9. W. V. Bhat, J. F. Wilby "Interior noise radiated by an airplane fuselage subjected to turbulent boundary layer excitation and evaluation of noise reduction treatments". J. Sound and Vibration 18, 4, 449-464 (October 1971).

10. R. P. Goss "Acoustic program for the Grumman Gulfstream II". AIAA Paper 71-783. AIAA 3rd Aircraft Design and Operation Meeting, Seattle (July 1971).

11. G. T. Gehhardt "Acoustical design features of Boeing Model 727". J. Aircraft 2, 4, 272-277 (July - August 1965).

12. T. J. Schultz "Wrappings, enclosures and duct linings". Chp 15 of Noise and Vibration Control. Editor L. L. Beranek, McGraw-Hill (1971).

13. L. D. Jacobs, D. R. Lagerquist "A finite element analysis of simple panel response to turbulent boundary layers". AFFDL-TR-67-81 (July 1967).

14. J. F. Wilby "The response of simple panels to turbulent boundary layer excitation". AFFDL-TR-67-70 (1967).

15. D. J. Mead "The damping of stiffened plate structures". Chp 26 of Acoustic Fatigue in Aerospace Structures. Edited by W. J. Trapp, D. M. Forney, Syracuse University Press (1965).

16. D. J. Mead, E. J. Richards, Editors, "Noise and Acoustic Fatigue in Aeronautics". John Wiley and Sons Inc. (1968).

17. L. D. Jacobs, D. R. Lagerquist "Finite-element analysis of complex panel response to random loads". AFFDL-TR-68-144 (April 1968)

18. J. F. Wilby, F. L. Gloyna "Vibration measurements of an airplane fuselage structure, I. Turbulent boundary layer excitation". J. Sound and Vibration. 23, 4, 443-466 (August 1972).

19. J. A. Hay "Experimentally determined damping factors". Chp 12 of Symposium on Acoustic Fatigue, AGARD-CR-113 (May 1973).

20. P. A. Franken, R. H. Lyon "Estimation of sound-induced vibrations by energy methods, with applications to the Titan Missile". The Shock and Vibration Bulletin, No. 31, Part III 12-26 (April 1963).

21. J. E. Manning, R. H. Lyon, T. D. Scharton "Transmission of sound and vibration to a shroud-enclosed spacecraft". NASA-CR-81688 (October 1966) (Also BBN Report 1431).

22. W. F. Stokey "Vibration of systems having distributed mass and elasticity". Vol 1, Chp 7 of Shock and Vibration Handbook. Editors C. M. Harris, C. E. Crede, McGraw-Hill (1961).

23. A. W. Leisson "Vibration of Shells". NASA-SP-288 (1973).

24. J. F. Wilby, F. L. Gloyna "Vibration measurements of an airplane fuselage structure, II Jet noise excitation". J. Sound and Vibration, 23, 4, 467-486 (August 1972).

25. T. D. Scharton "Response of a ring-stringer stiffened cylinder to acoustical and mechanical excitation". NASA CR-103172 (April 1971) (Also BBN Report 1997).

26. A. J. Price, M. J. Crocker "Sound transmission through double panels using statistical energy analysis". J. Acous. Soc. Amer., 47, 3 (Part 1) 683-693 (March 1970).

27. T. D. Scharton, T. M. Yang "Statistical energy analysis of vibration transmission into an instrument package". Paper 670876, SAE Meeting, Los Angeles (October 1967).

28. R. H. Lyon, E. Eichler "Random vibration of connected structures". J. Acous. Soc. Amer., 36, 7, 1344-1354 (July 1964).

29. P. R. Nayak "Line admittance of infinite isotropic fluid-loaded plates". J. Acous. Soc. Amer., 47, 1, (Part 2), 191-201 (January 1970).

30. I. L. Vér, C. I. Holmer "Interaction of sound waves with solid structures". Chp 11 of Noise and Vibration Control. Editor L. L. Beranek, McGraw-Hill (1971).

31. R. E. Hayden, T. D. Scharton, Y. Kadman, J. Wilby and M. J. Rudd, "A Preliminary Evaluation of Noise Reduction Potential for the Upper Surface Blown Flap," BBN Report No. 2478, submitted to NASA Langley Research Center on 7 November 1973.

32. B. J. Clark, R. G. Dorsh and M. Reshotko, "Flap Noise Prediction Method for a Powered Lift System," AIAA Paper No. 73-1028, presented in AIAA Aero-Acoustics Conference, Seattle, Washington, October 15-17, 1973.

33. M. D. Falarski, K. Aoyagi, and D. Koenig,""Acoustic Characteristics of a Large-Scale Wind-Tunnel Model of an Upper-Surface Blown Flap Transport Having Two Engines," NASA TM-X-62-319, NASA Ames Research Center, September 1973.

34. T. Scharton, B. Pinkel, J. Wilby and G. L. Hansen, "A Study of Trailing Edge Blowing as a Means of Reducing Noise Generated by the Interaction of Flow with a Surface," BBN Report No. 2593, submitted to NASA Langley Research Center, 1 June 1974.

35. T. Scharton, P. White, P. Rentz, "Supersonic Jet Noise Investigation Using Jet Fluctuating Pressure Probes," BBN Report No. 2220, submitted to Air Force Aeropropulsion Laboratory June 1972 under Contract No. F33615-71-C-1661.

36. D. M. Chase "Noise Radiated from an Edge in Turbulent Flow According to a Model of Hydrodynamic Pressure; Comparison with a Jet-Flow Experiment," AIAA Paper No. 74-570, presented at AIAA 7th Fluid and Plasma Dynamics Conference, June 18, 1974.

37. R. E. Hayden, "Fundamental Aspects of Noise Reduction from Powered-Lift Devices," SAE Paper No. 730376, presented at Air Transportation Meeting, April 24-26, 1973.

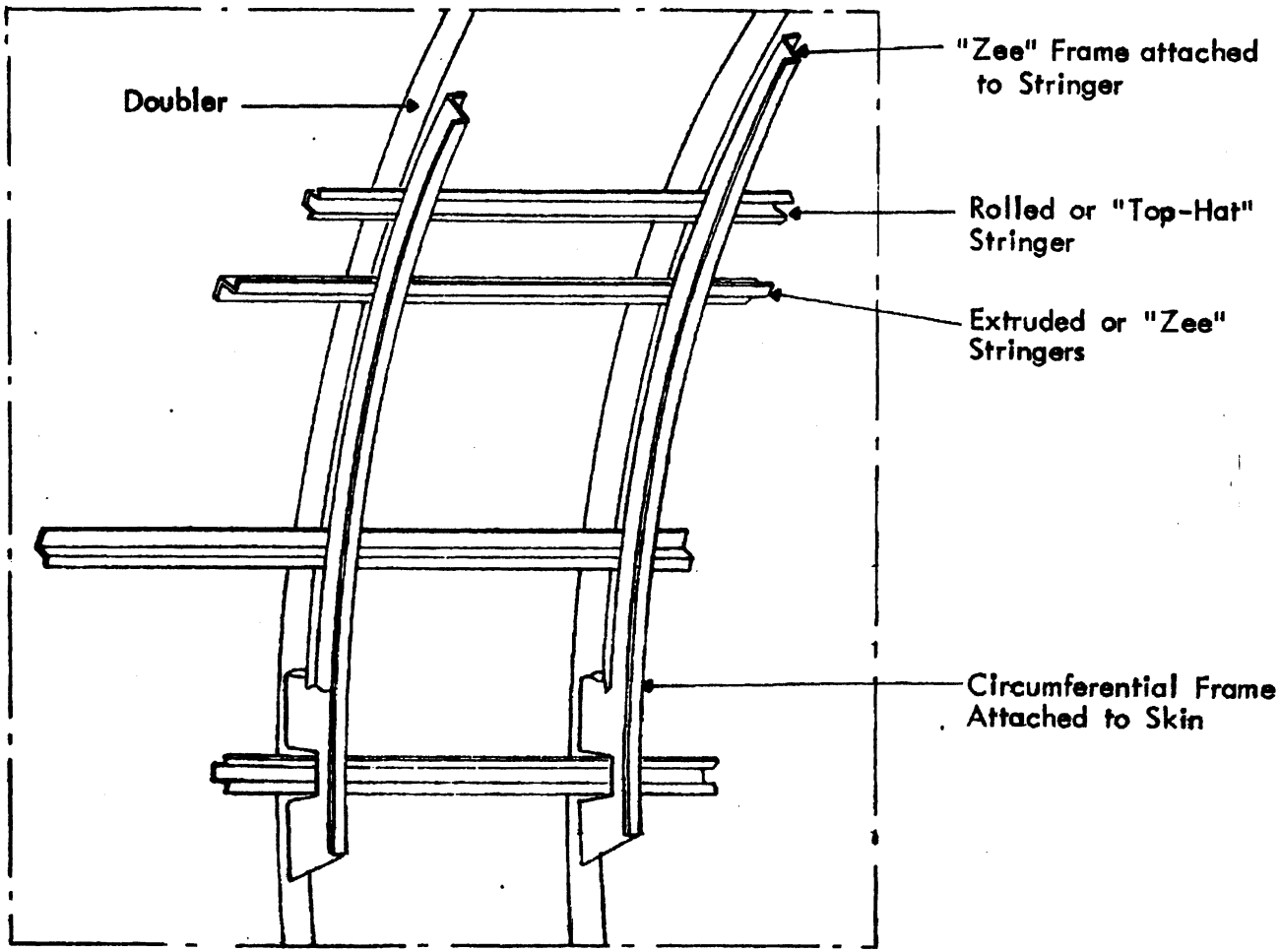

FIGURE 1. TYPICAL FUSELAGE CONSTRUCTION

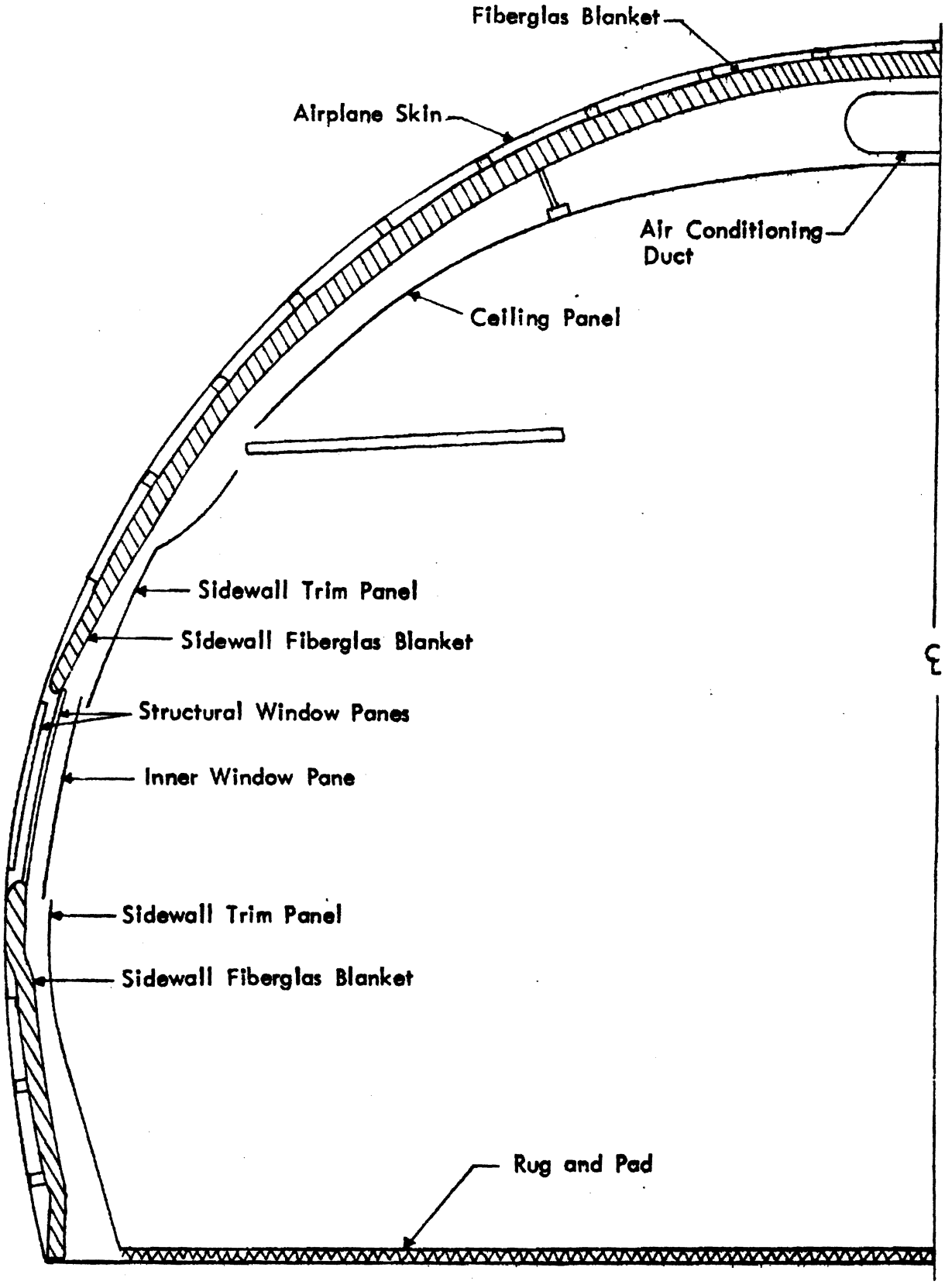

FIGURE 2. TYPICAL AIRPLANE SIDEWALL CONSTRUCTION

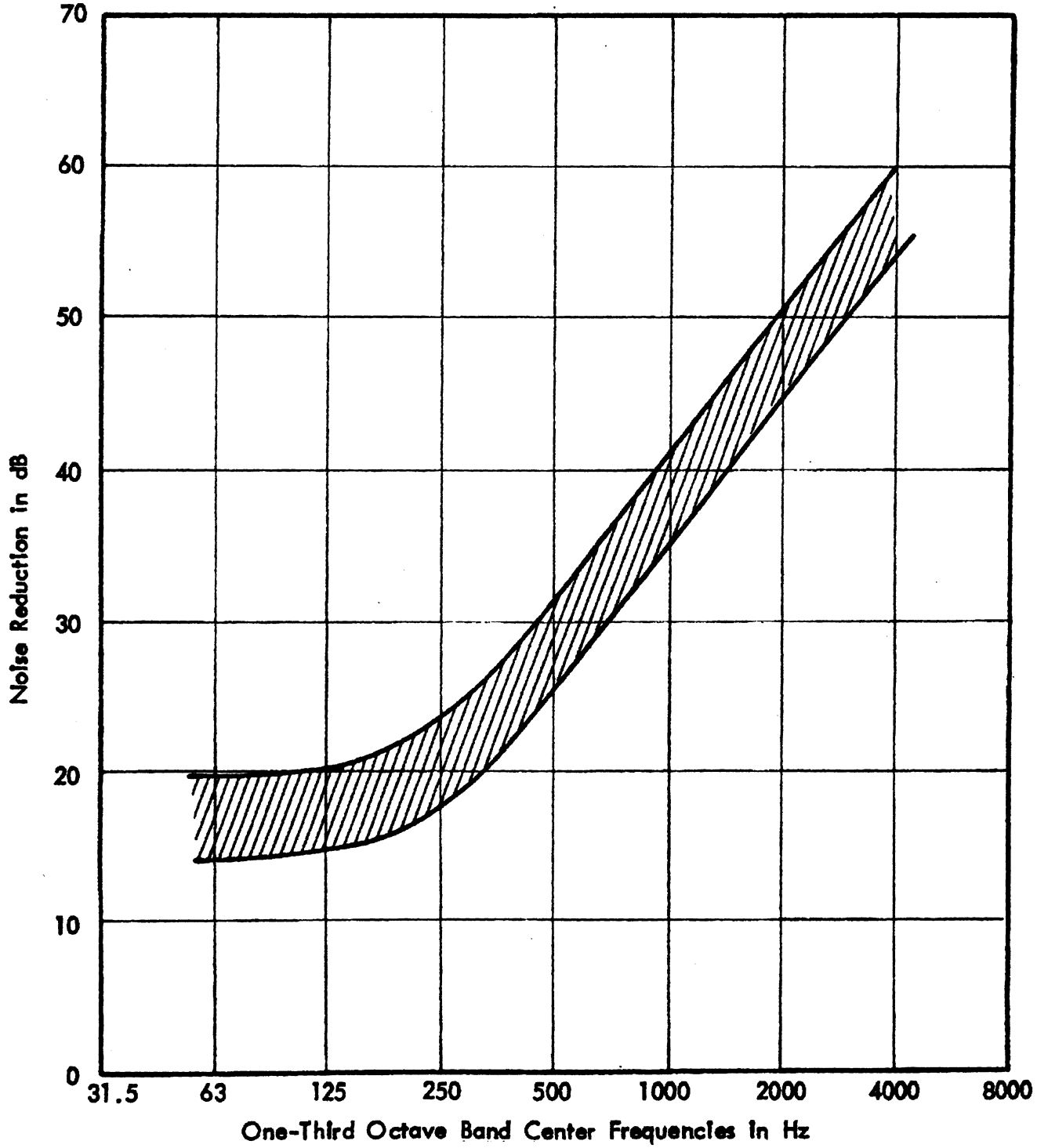

FIGURE 3. EMPIRICAL NOISE REDUCTION SPECTRUM FOR CONVENTION AIRPLANE FUSELAGE

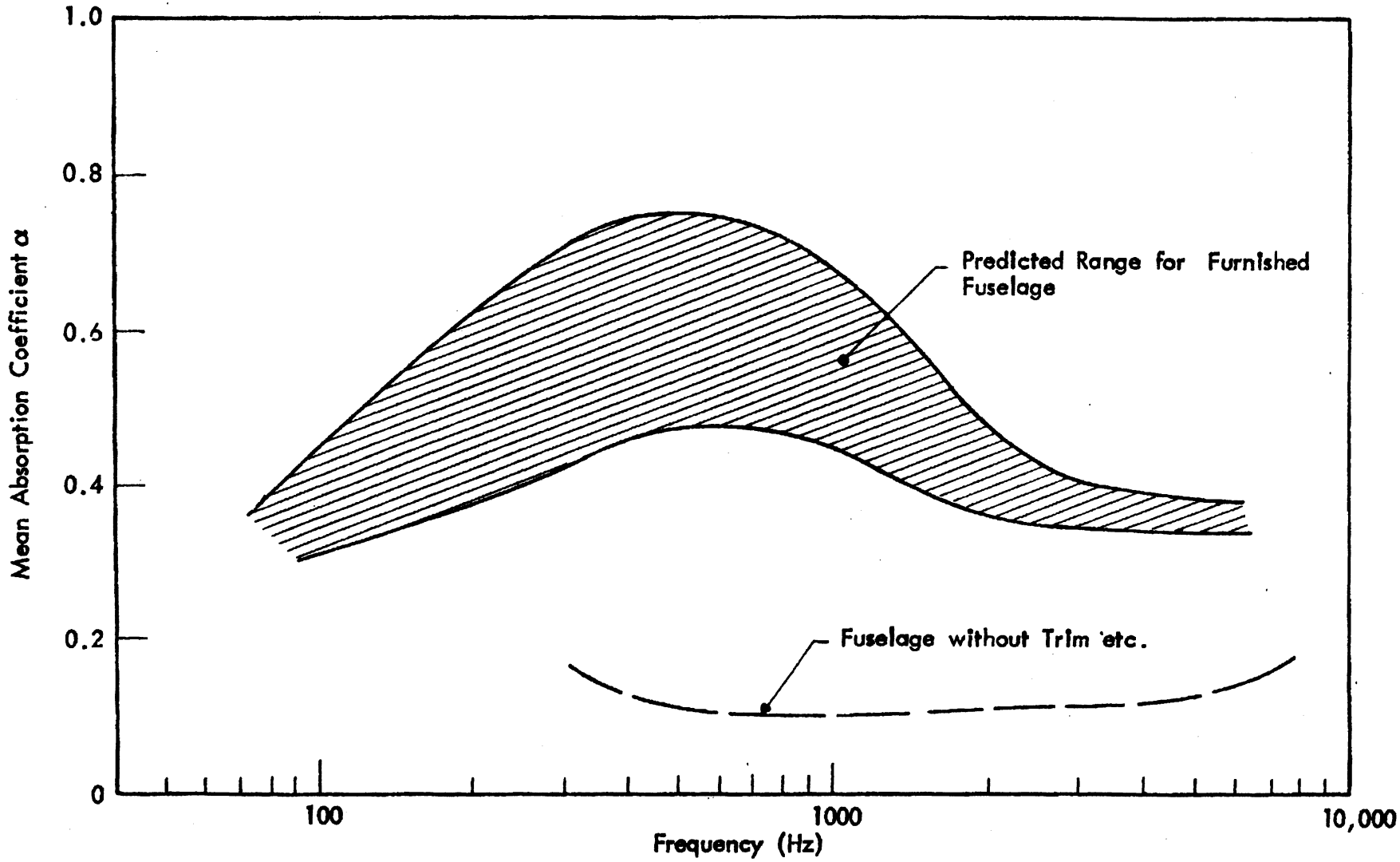

FIGURE 4. MEAN ABSORPTION COEFFICIENTS FOR FUSELAGE INTERIOR

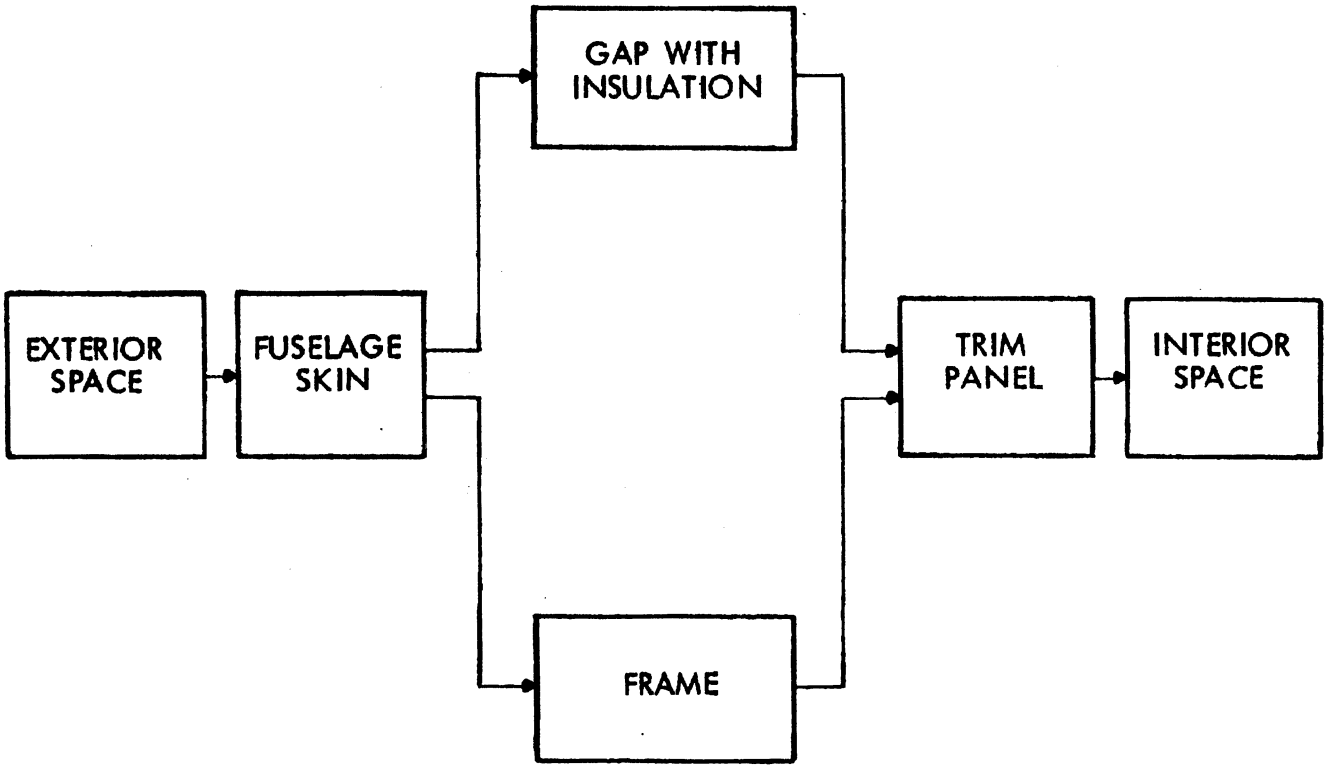

FIGURE 5. ENERGY FLOW DIAGRAM FOR FUSELAGE SIDEWALL MODEL

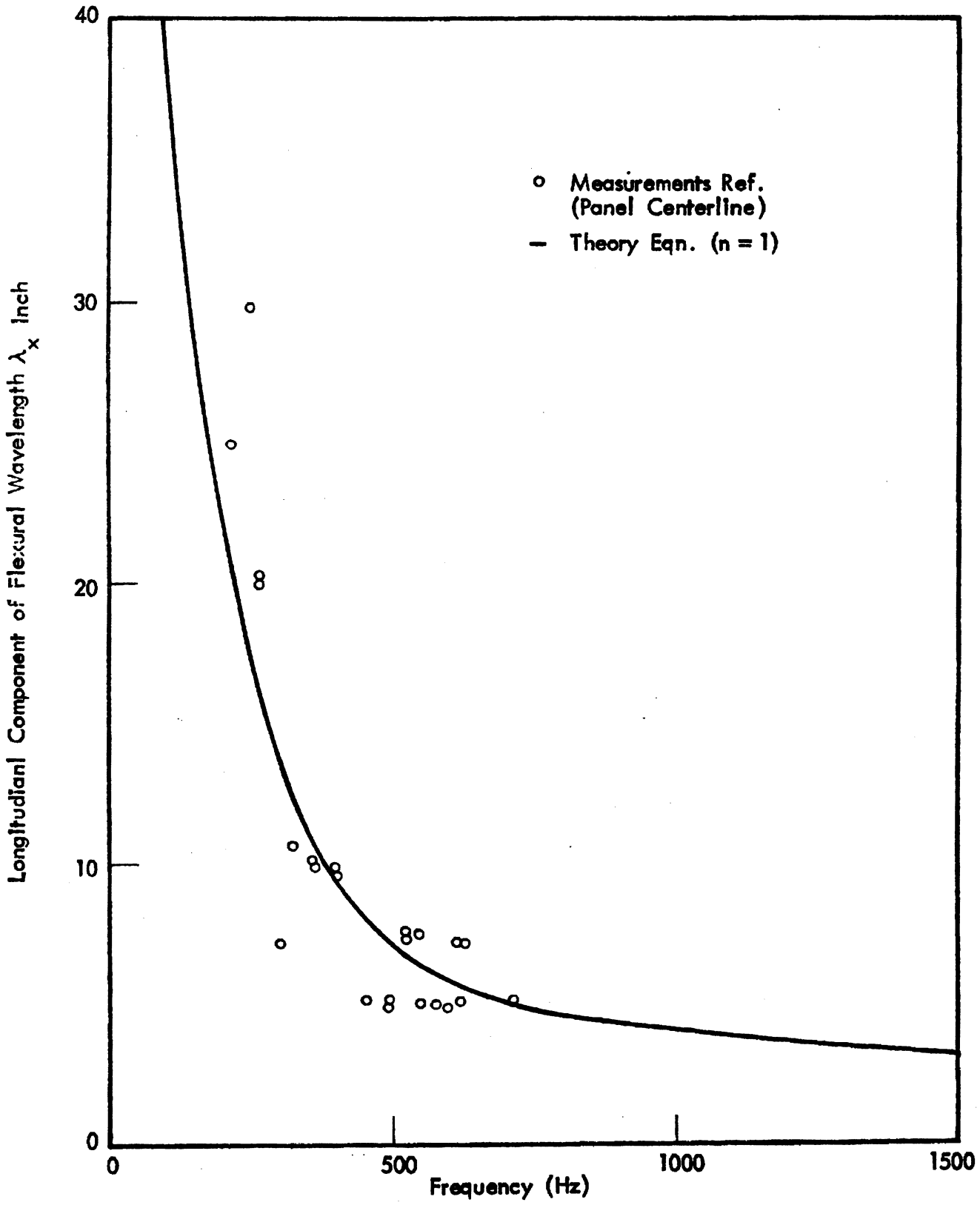

FIGURE 6. FLEXURAL WAVELENGTH FOR FUSELAGE SKIN PANEL

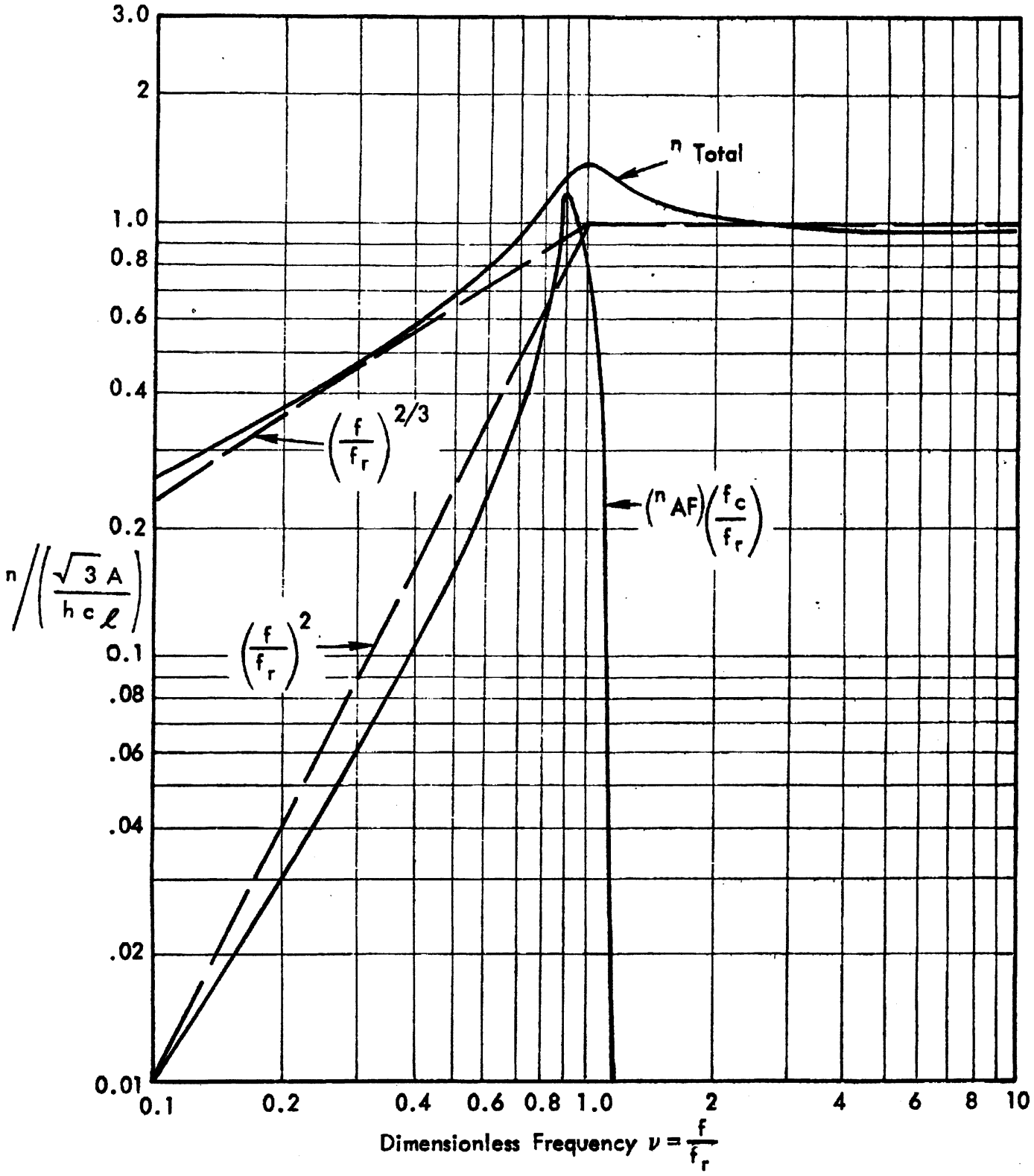

FIGURE 7. ONE-THIRD OCTAVE BAND AVERAGE MODAL DENSITIES FOR A CYLINDER

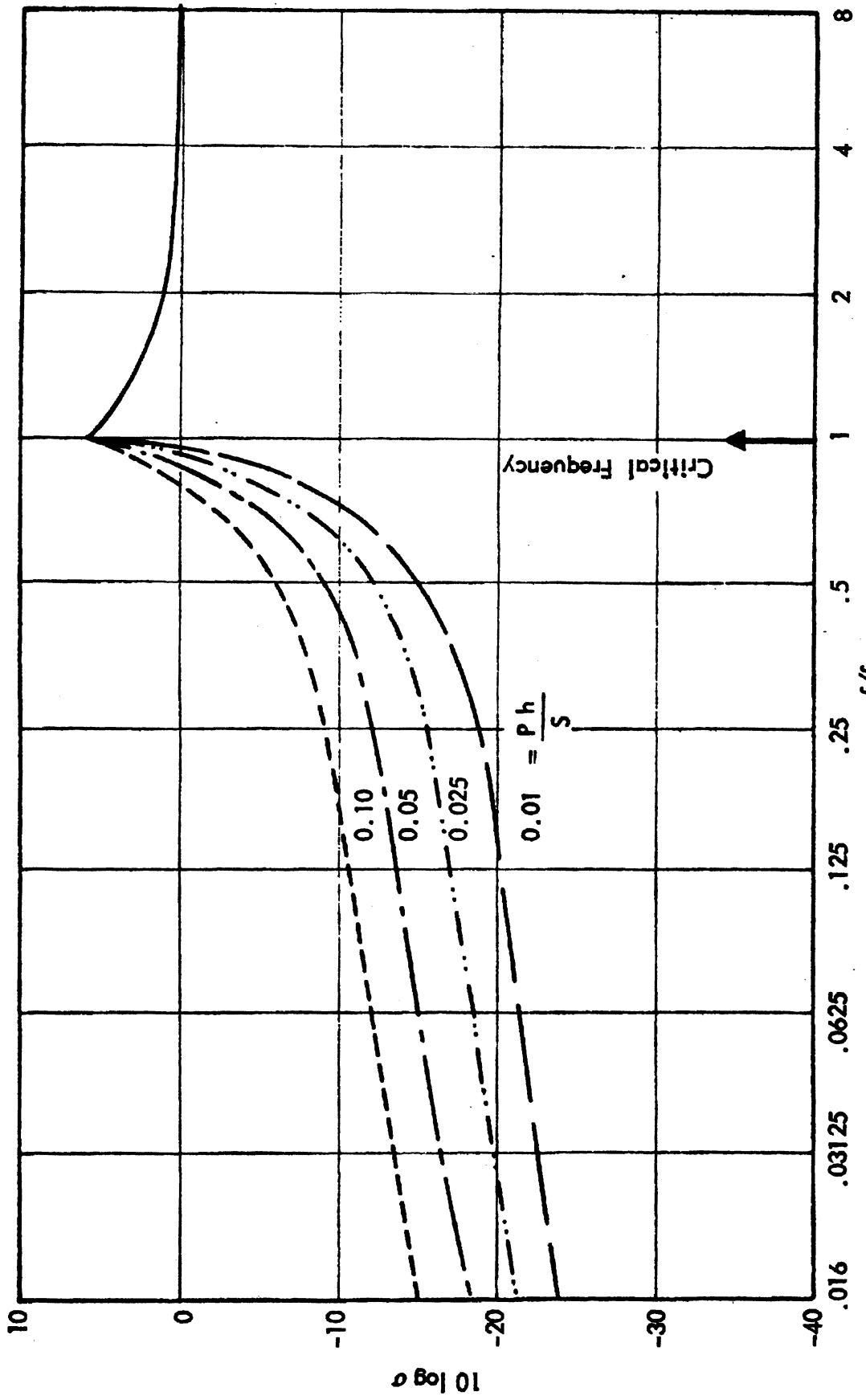

FIGURE 8. RADIATION EFFICIENCY OF STEEL AND ALUMINUM FLAT PANELS (SIMPLE SUPPORTED EDGES)

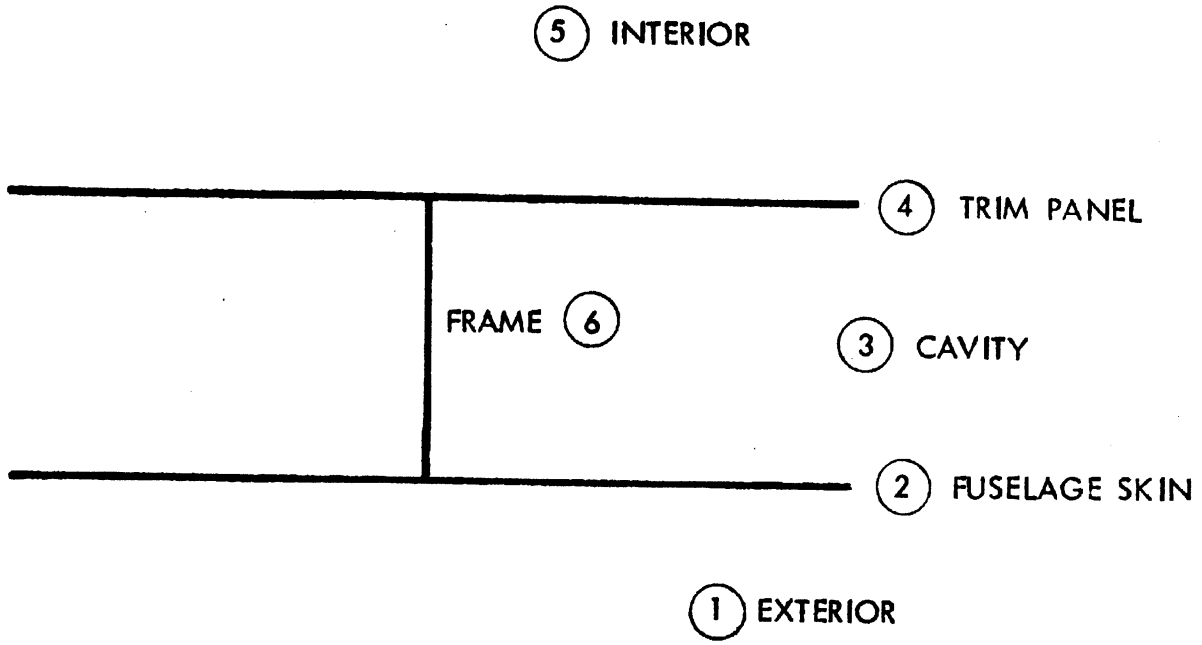

FIGURE 9. REPRESENTATION OF SIDE WALL

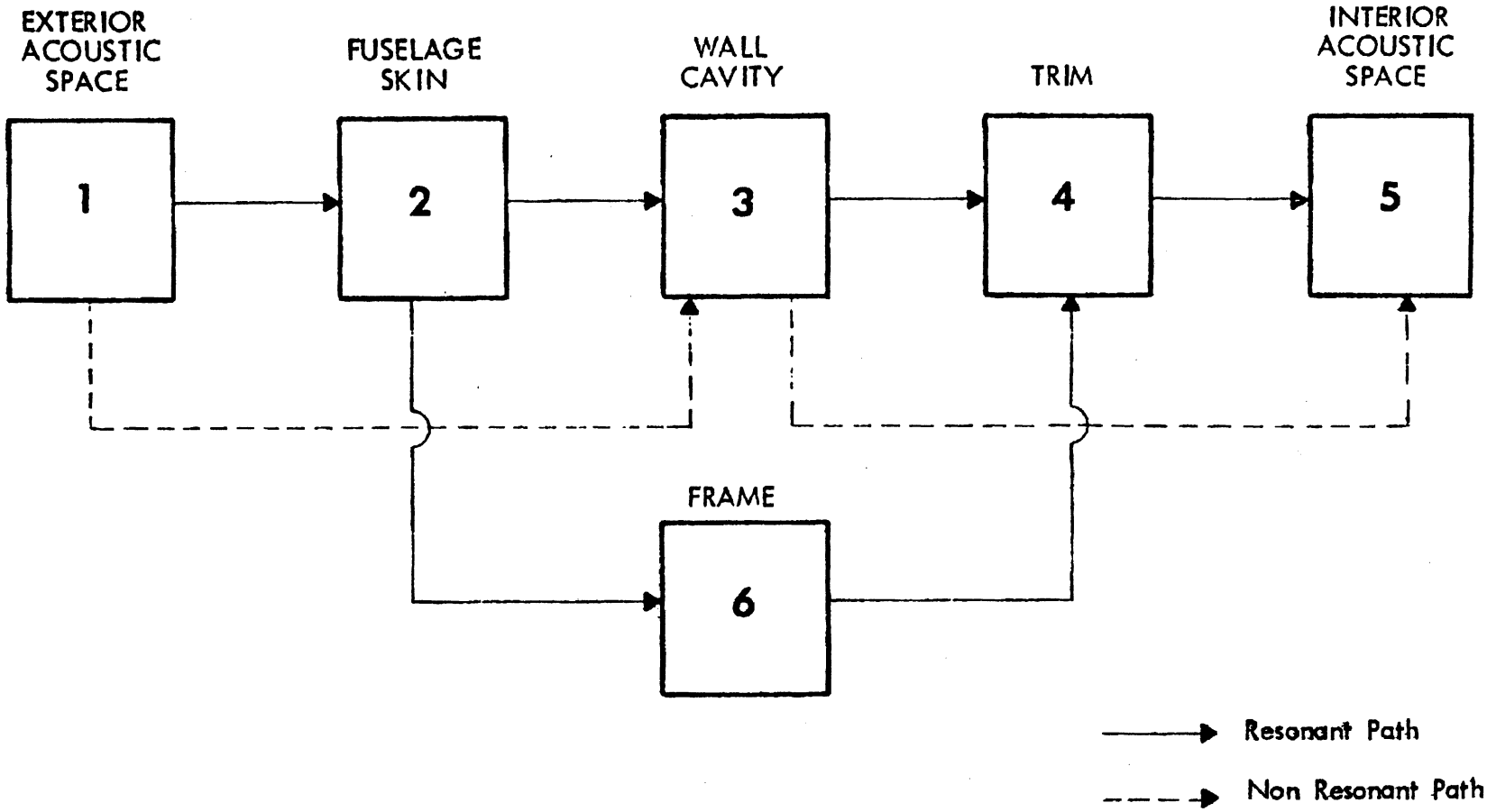

FIGURE 10. ENERGY FLOW PATHS

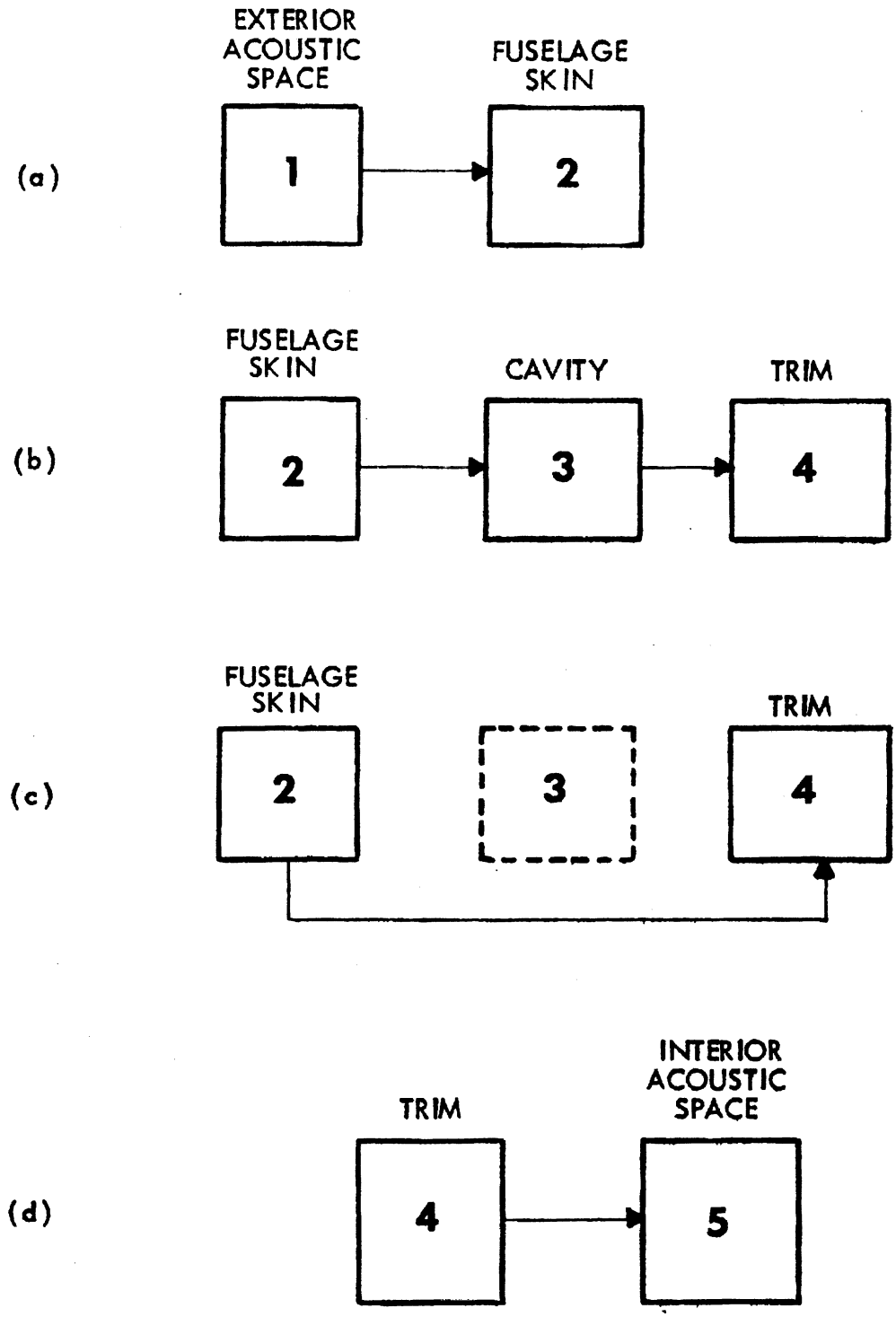

FIGURE 11. ENERGY FLOW PATHS FOR RESONANT COMPONENT SYSTEMS

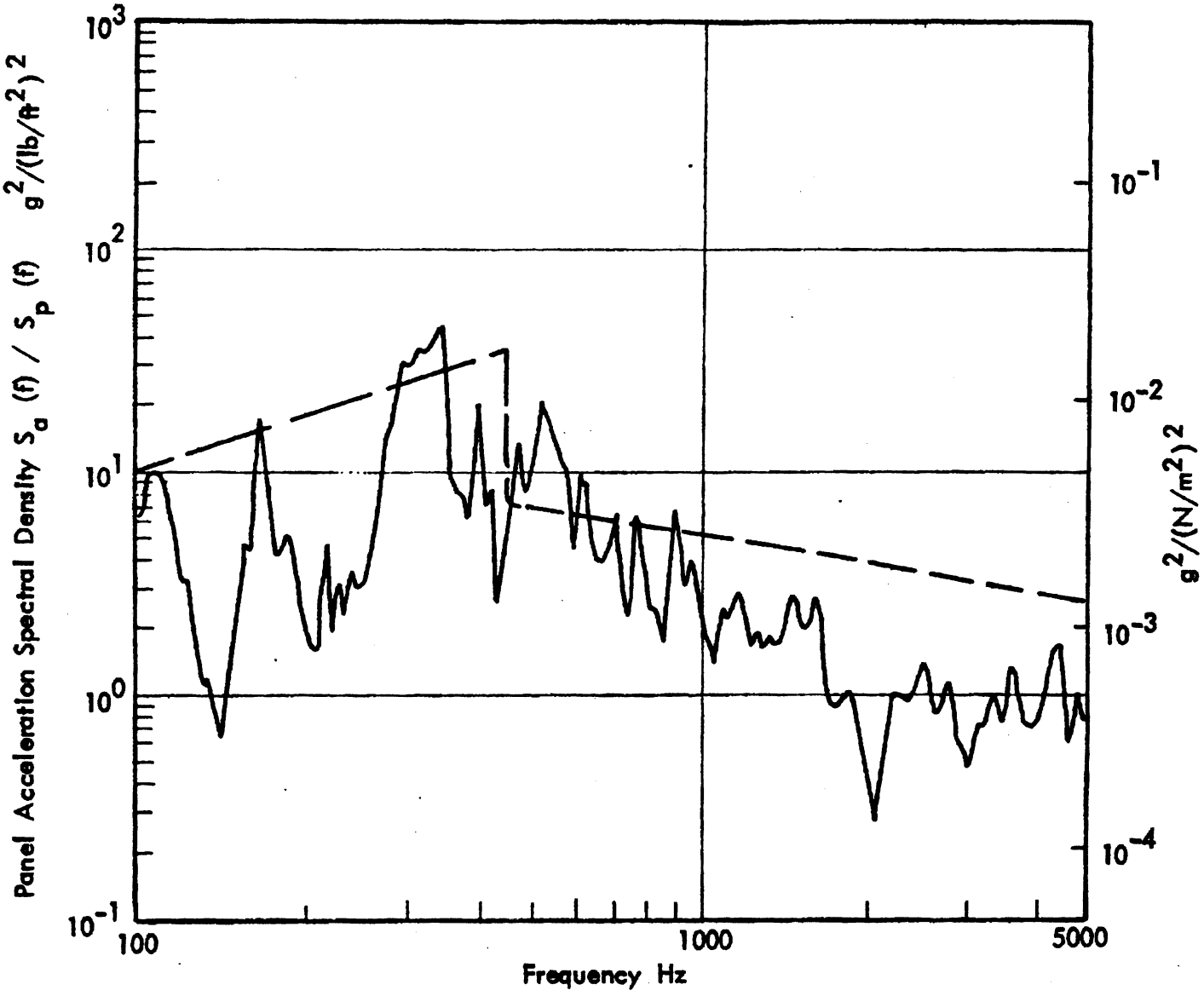

FIGURE 12. MEASURED AND PREDICTED FUSELAGE SKIN VIBRATION

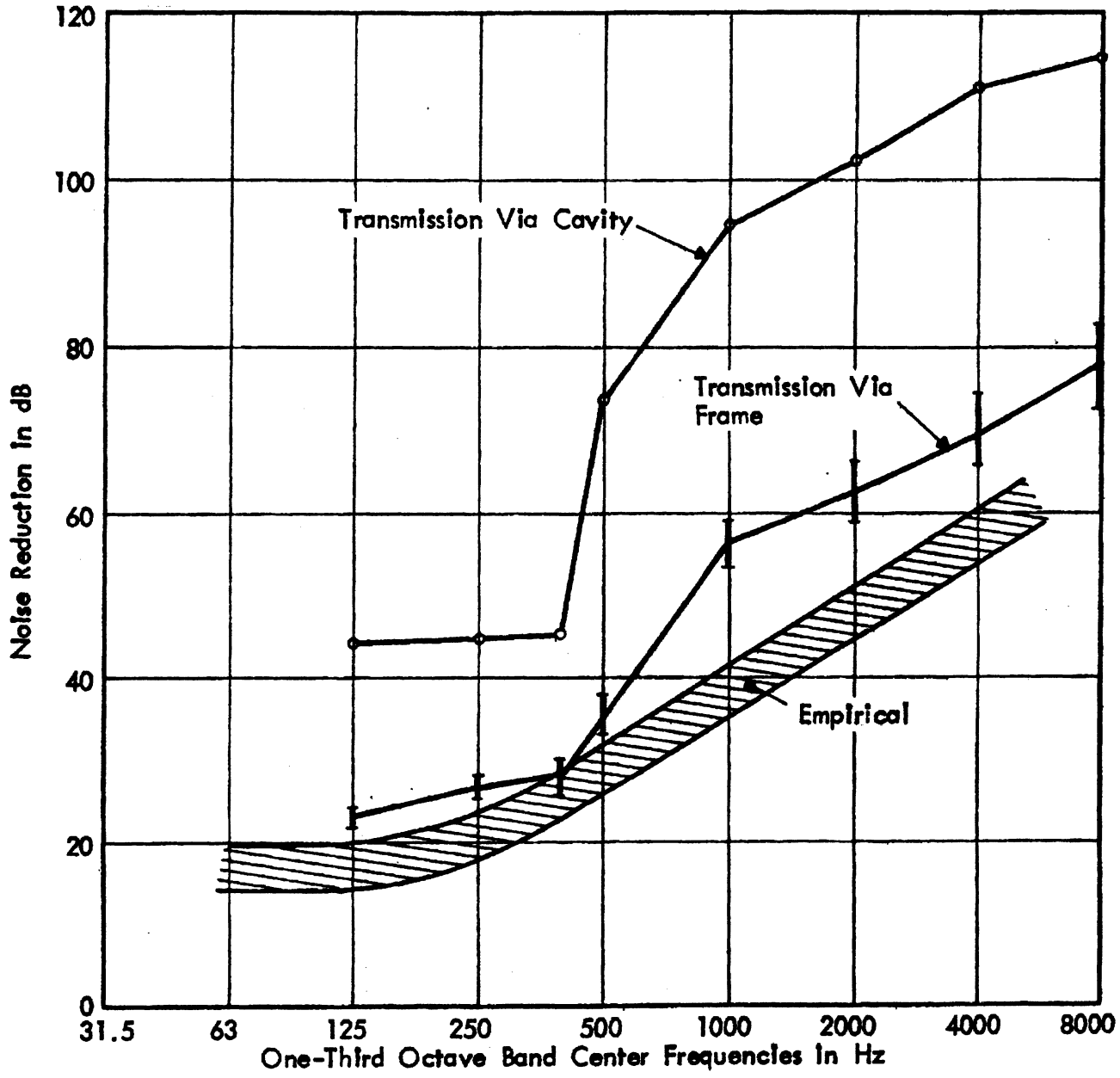

FIGURE 13. NOISE REDUCTION PREDICTED BY PANEL RESONANT RESPONSE ANALYSIS

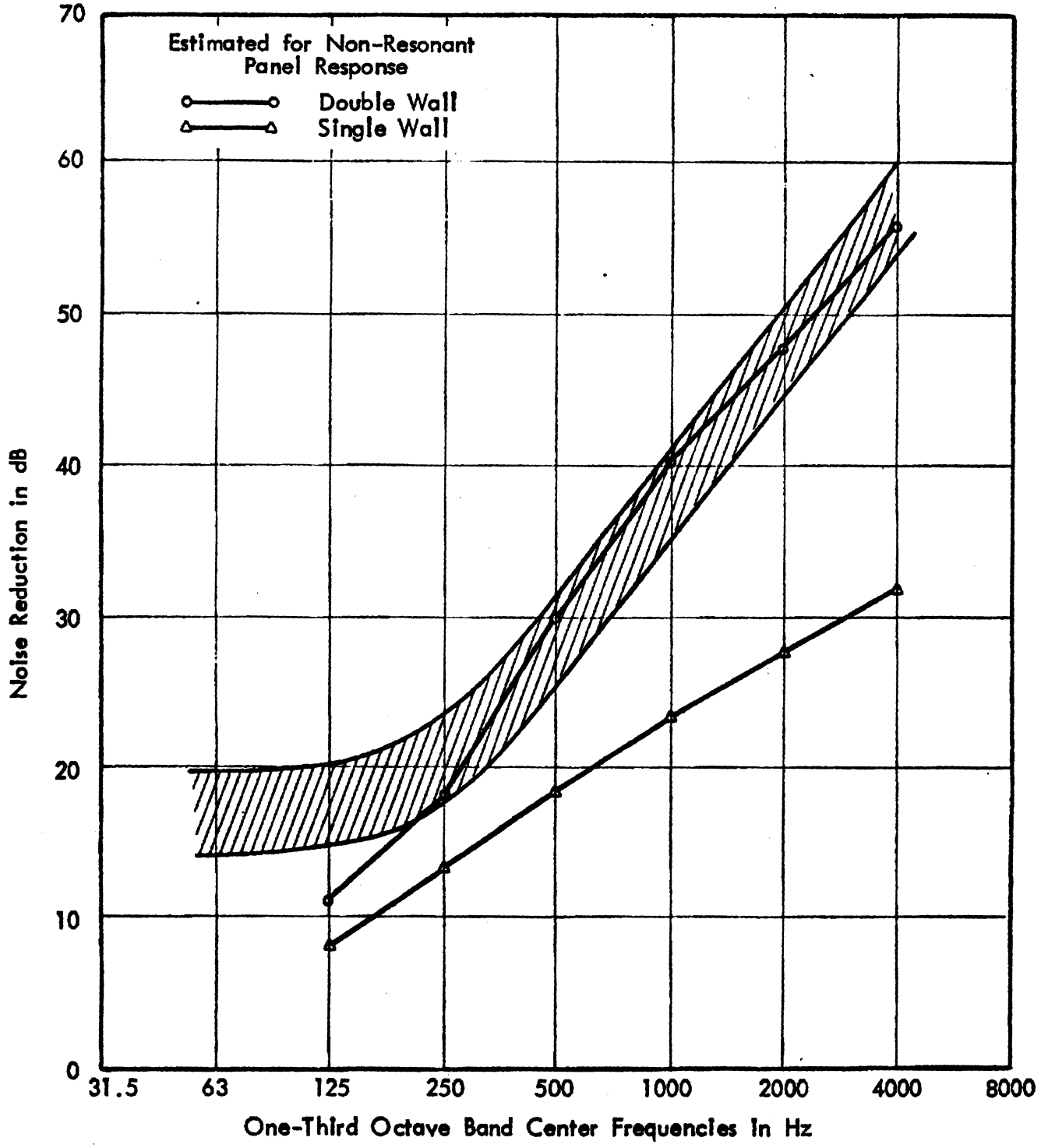

FIGURE 14. NOISE REDUCTION PREDICTED BY PANEL NON-RESONANT RESPONSE ANALYSIS

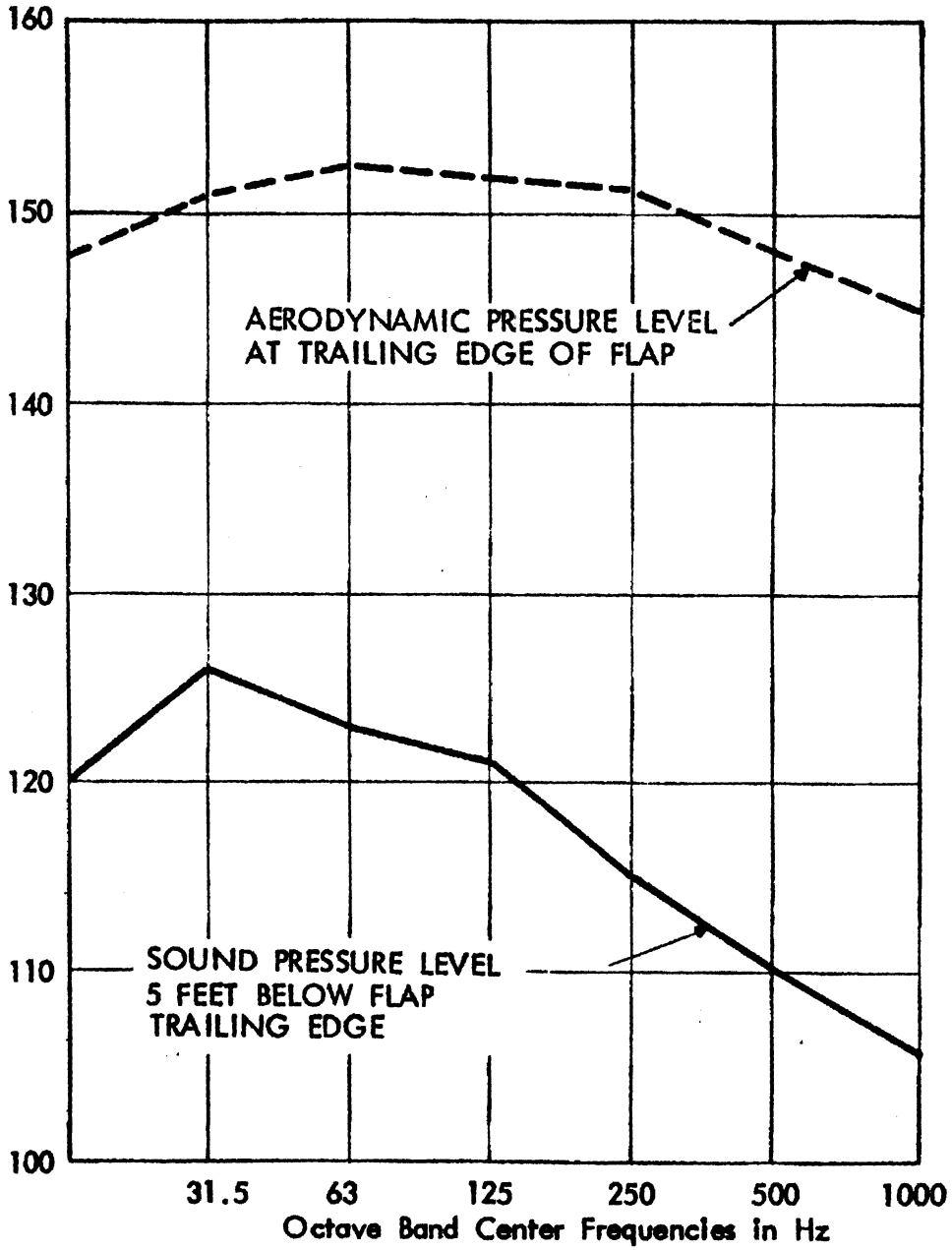

DATA SOURCE:

BBN 1/15th Scale Model Tests (BBN Report 2478 Submitted LRC, 7 November 1972)

ASSUMPTIONS:

1. One Engine Contributes
2. Jet Velocity = 800 ft/sec, Thrust = 21,000 lb.
3. Ratio of Nozzle Width to Height Equal to 10, Ratio of Nozzle Exit to Trailing Edge Distance to Nozzle Height Equal to 15.
4. Jet at Std. Atmospheric Temperature and Denity
5. Forward Speed Zero

FIGURE 15. EXTERIOR ACOUSTIC AND AERODYNAMIC FLUCTUATING PRESSURE SPECTRA FOR USB QCSEE TWO ENGINE AIRCRAFT

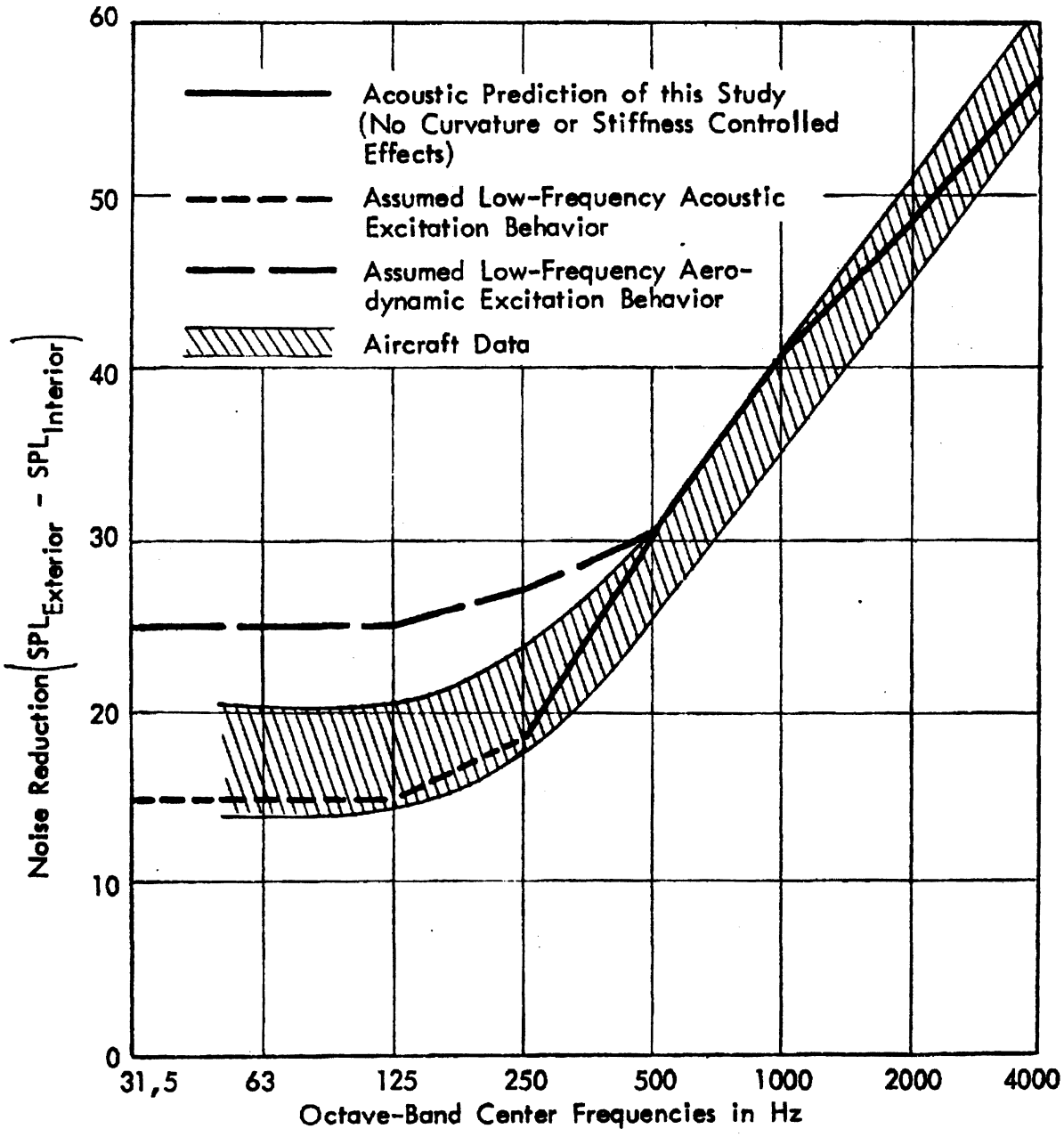

FIGURE 16. FUSELAGE NOISE REDUCTION

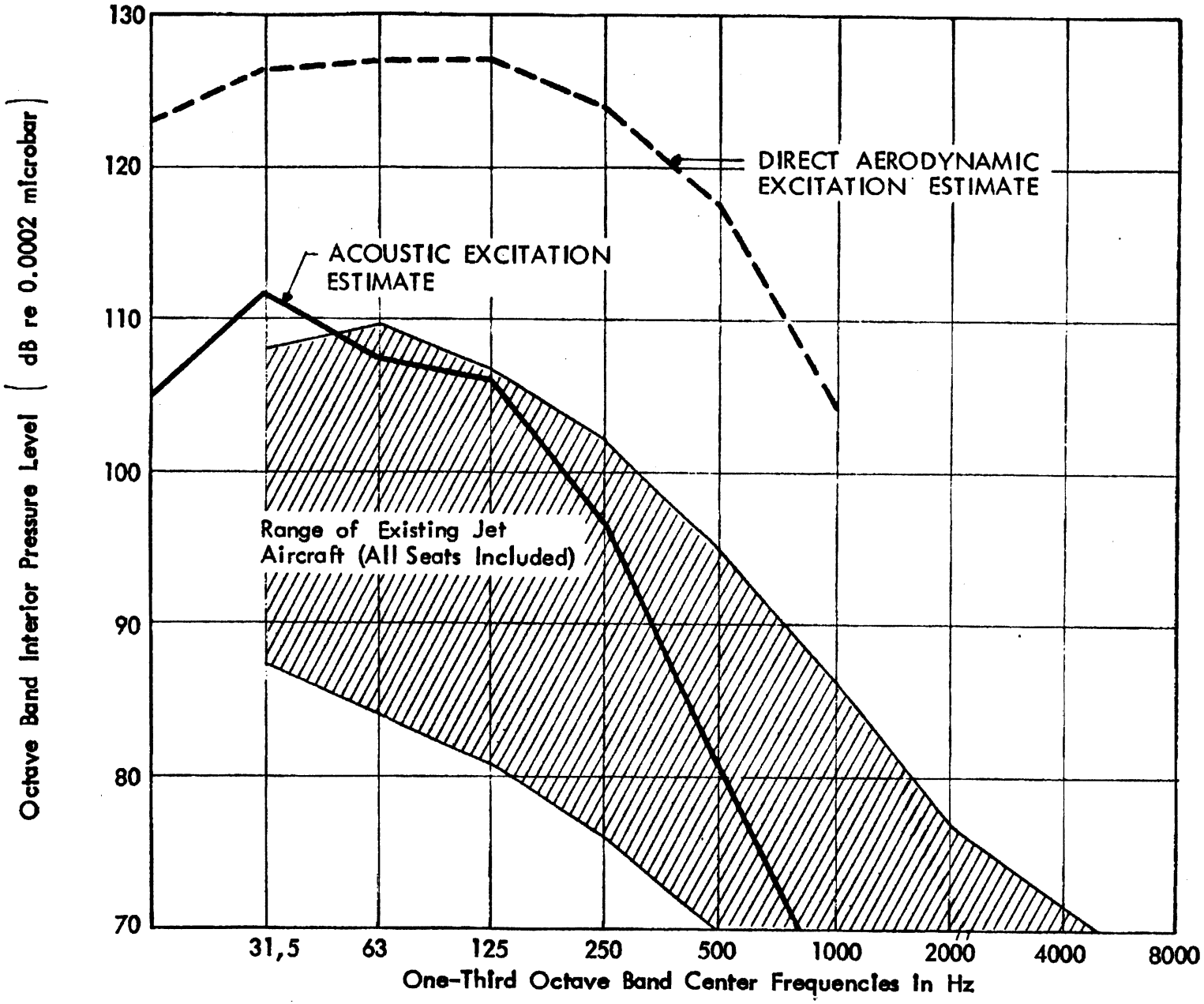

FIGURE 17. COMPARISON OF OWB AIRCRAFT INTERIOR NOISE ESTIMATES WITH DATA FOR CURRENT JET AIRCRAFT

Appendix A

Acoustic Absorption Inside Fuselage

Main contributors to the acoustic absorption in the passenger compartment are the sidewall trim panel, ceiling panels, bulkheads, seats, and rug and pad. The presence of passengers will change the absorptive properties since the passengers will increase absorption but will shield the seats thereby reducing the acoustic energy absorbed by the seats. The net effect of the passengers will probably be a small increase in absorption[A.1]. A compartment without passengers will be considered in this study.

The floor of a passenger compartment is covered with a rug and pad which provide acoustic absorption. The effectiveness of the rug and pad can be estimated from published data on similar materials. Such data are listed in Table A.1, and a mean value for the absorption coefficient is shown at each frequency.

Table A.1
Acoustic Absorption Coefficients for Rug and Pad

Frequency (Hz)	125	200	350	500	1000	2000	4000
Description:							
Theater carpet [A.2]			0.13	0.185	0.39	0.50	0.565
3/8-inch woolpile on concrete [A.3]		0.08		0.21	0.26	0.27	0.37
Short uncut woolpile on 1/4-inch sponge [A.1]	0.06		0.13	0.37	0.41	0.46	0.55
Tufted nylon on 1/4-inch sponge [A.1]	0.06		0.14	0.34	0.36	0.31	0.37
Average α_R	0.06	0.08	0.13	0.28	0.36	0.39	0.46

Absorption provided by seats is taken from measurements on upholstered foam rubber seats covered with woven fabric [A.1]. Measurements were made in the laboratory using ten chairs so that shielding effects of adjacent seats would be included. Data shown in Table A.2 show the absorption A_s per chair in Sabines. To convert into an equivalent absorption coefficient α_s an area S_s of enclosure wall is assigned to each seat. For narrow-body fuselages typical of Boeing 707 and Douglas DC-8 airplanes, S_s is approximately 16.6 sq. ft. and for wide-body fuselages typical of Boeing 747, S_s = 18.2 sq. ft. Table A.2 shows equivalent absorption coefficients estimated for each fuselage size and a value averaged over both fuselage sizes.

Table A.2
Acoustic Absorption Coefficients for Seats

Frequency (Hz)	125	250	500	1000	2000	4000
Description:						
Absorption A_s of unoccupied seat [A.1] Sabines	2.4	2.8	3.5	3.2	2.7	2.6
$\alpha_s = A_s/S_s$ Narrow fuselage	0.14	0.17	0.21	0.19	0.16	0.16
Wide-body fuselage	0.13	0.15	0.19	0.18	0.15	0.14
Average α_s	0.14	0.16	0.20	0.18	0.16	0.15

Estimation of absorption coefficients for the sidewall and ceiling trim panels is difficult because of the scarcity of representative data and the variety of trim panel designs in current use. For glass-fiber blankets covered with unperforated vinyl Nichols et al [A.4] measured absorption coefficients shown in Table A.3. Diaphragm action of the vinyl provides high absorption coefficients at lower frequencies but the absence of perforations reduces high frequency absorption. Trim panels which are more rigid will probably provide similar high frequency absorption but the low frequency coefficients may be lower than those shown in Table A.3.

Table A.3

Absorption Coefficients for Trim Panels

Frequency (Hz)	200	350	500	1000	2000	4000
Vinyl-covered glass-fiber blankets α_T	0.7	0.74	0.73	0.57	0.25	0.13

Absorption coefficients for trim panel, seats, and rug and pad are compared in Figure A.1. The coefficients can be combined to determine an average absorption coefficient α for the compartment, where

$$\alpha = \frac{S_T}{S} \alpha_T + \frac{S_R}{S} \alpha_R + \alpha_S \qquad (A.1)$$

In equation (A.1), S_T and S_R are the surface areas of the trim and floor respectively, and

$$S = S_T + S_R \qquad (A.2)$$

Equation (A.1) assumes that the influence of the bulkheads is small since the area forms a small fraction of the total surface area in a typical passenger compartment. If the assumption were not true a fourth term $\frac{S_B}{S} \alpha_B$ would have to be included on the right hand side of equation (A.1) and equation (A.2) would become

$$S = S_T + S_R + S_B$$

From data on typical airplanes

$$\frac{S_R}{S} \approx 0.35, \quad \frac{S_T}{S} \approx 0.65 \qquad (A.3)$$

and equation (A.1) becomes

$$\alpha = 0.65\ \alpha_T + 0.35\ \alpha_R + \alpha_S \qquad (A.4)$$

Evaluation of equation (A.4), using data in Figure A.1 provides an estimate of the mean absorption in a fully-furnished fuselage interior. The mean coefficients are shown in Figure A.2 as the upper limit of the hatched area. The lower boundary of the hatched region in Figure A.2 was calculated on the assumption that the ceiling panels, which form about 25% of the total surface area, were non-absorbent and that the absorption coefficients for the sidewall trim were reduced by about 30% because of the use of sheet metal or glass-fiber.

Also shown in Figure A.2 for comparison are absorption coefficients measured in a fuselage without trim, seats, rug and pad [A.5]. The coefficients were determined from reverberation time measurements inside the fuselage. Thus, there is one important difference between the data for furnished and unfurnished

fuselages. In the unfurnished case, the absorption coefficients represent the net effect of absorption within the fuselage and transmission to the exterior, whereas, the results for the furnished fuselage are based on reverberant chamber measurements and represent only the absorption within the fuselage. Transmission of energy to the exterior could have a significant influence on the bare fuselage data but, for typical fuselage construction, the transmitted energy should be small when compared to that absorbed by the interior surfaces, except at low frequencies.

References

A.1 T. D. Northwood, E. J. Stevens "Acoustical design of the Alberta Jubilee Auditoria" J. Acous. Soc. Amer. 30, 6, 507-516 June 1958

A.2 R. N. Lane "Absorption Characteristics of upholstered theater chairs and carpets as measured in two auditoriums" J. Acous. Soc. Amer. 28, 1, 101-105 January 1956.

A.3 L. L. Beranek "Acoustics" McGraw-Hill (1954)

A.4 R. H. Nichols, Jr., H. P. Sleeper, Jr., R. L. Wallace, Jr., H. L. Ericson "Acoustical materials and acoustical treatments for aircraft" J. Acous. Soc. Amer. 19, 428-443, 1947.

A.5 W. V. Bhat, J. F. Wilby "Interior noise radiated by an airplane fuselage subjected to turbulent boundard layer excitation and evaluation of noise reduction treatments" J. Sound and Vibration, 18 4, 449-464 October 1971.

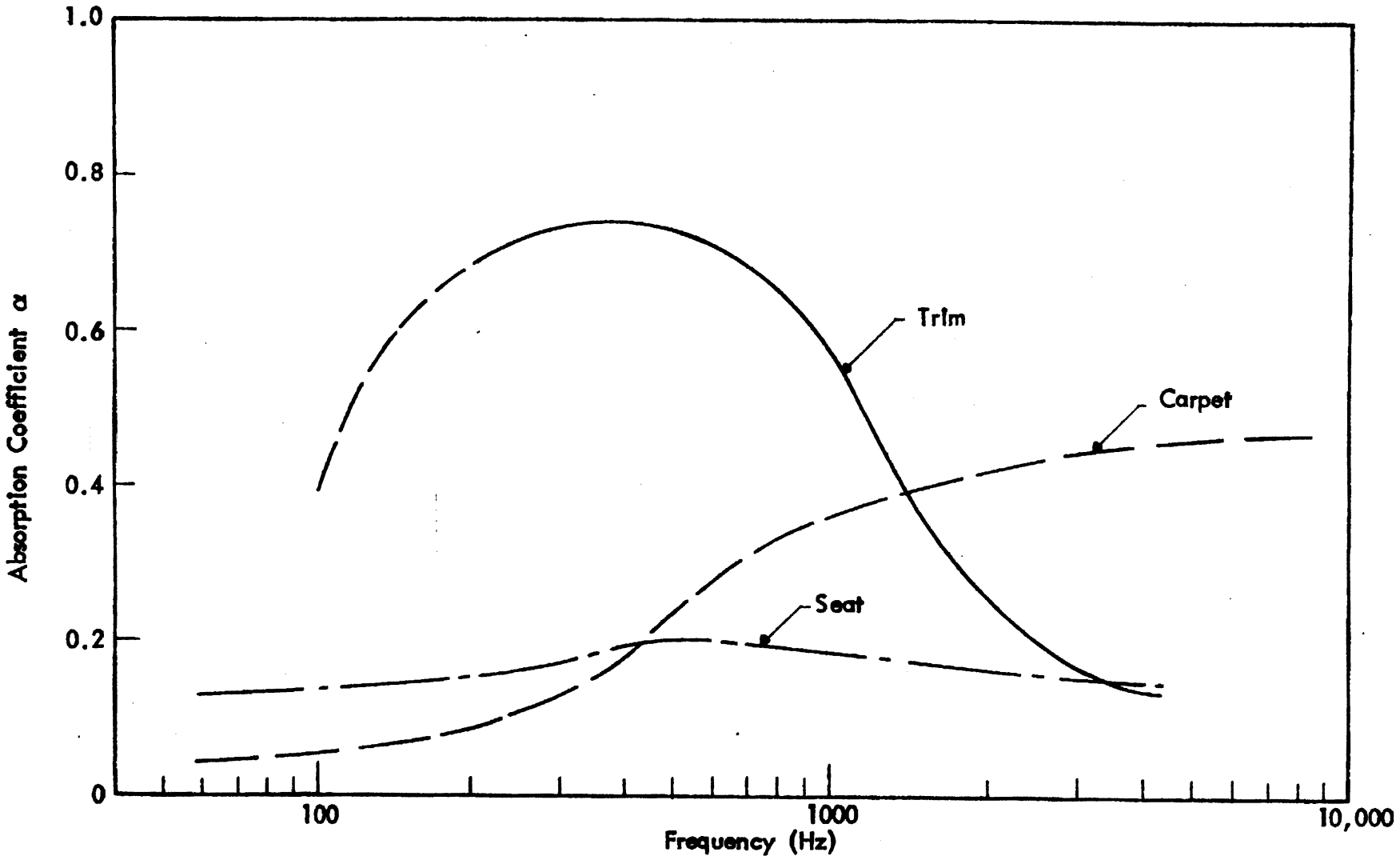

FIGURE A1. MEASURED ABSORPTION COEFFICIENTS FOR INTERIOR FURNISHINGS

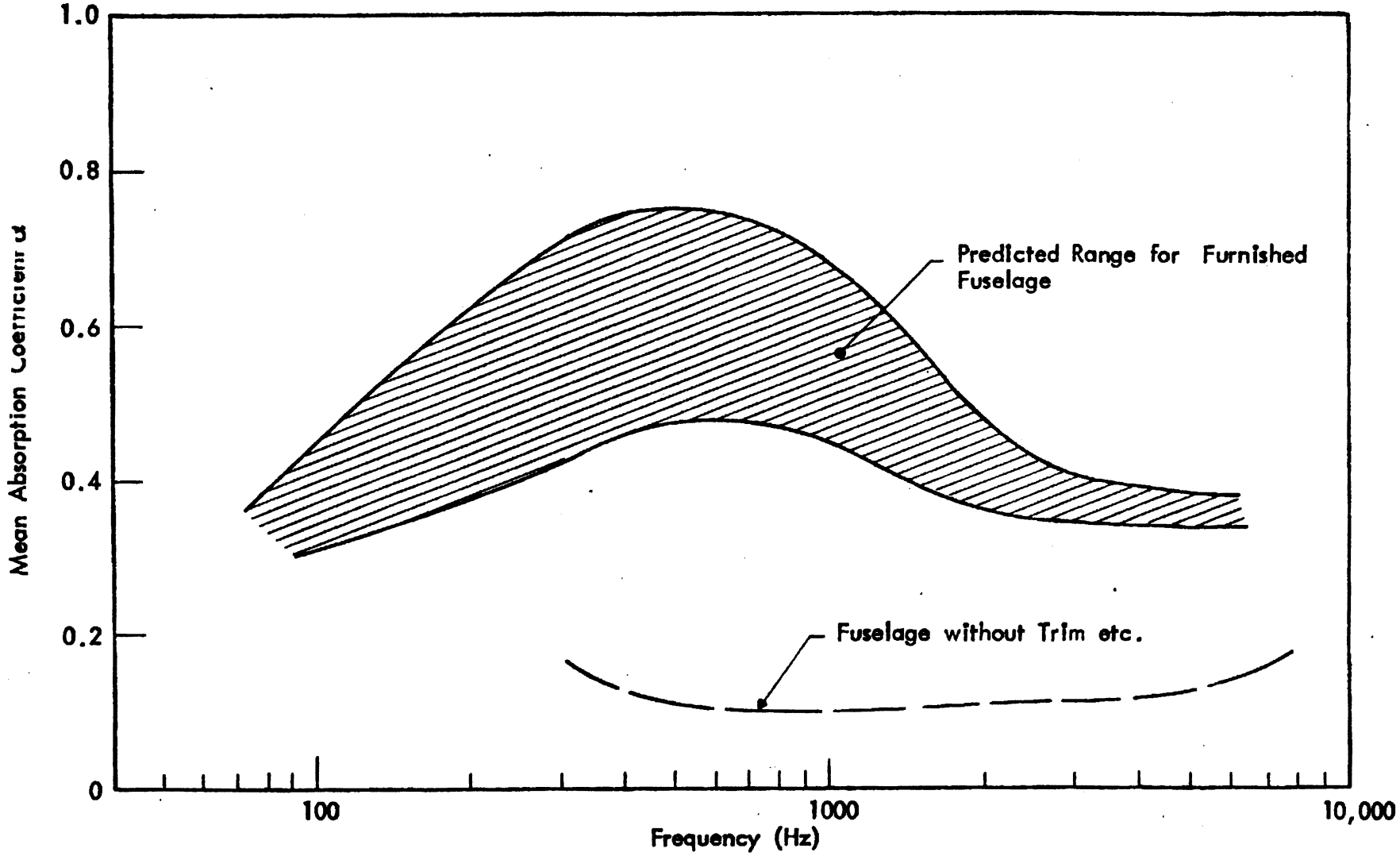

FIGURE A2. MEAN ABSORPTION COEFFICIENTS FOR FUSELAGE INTERIOR